Article

MFGE-8 identified in fetal mesenchymal-stromal-cell-derived exosomes ameliorates acute hepatic failure pathology

MSC-exosomes ameliorate AHF in mouse model

MFGE-8 found in exosome content based on proteomic analysis

The MFGE-8 protein managed to improve AHF liver phenotype

PI3K pathway emerged as molecular mediator in AHF progression in mice

Adriana Psaraki,
Dimitra Zagoura,
Lydia Ntari, ...,
Aristides G.
Eliopoulos,
Antonia Vlahou,
Maria G.
Roubelakis

roubel@med.uoa.gr

Highlights

EXO administration improved liver phenotype *in vivo* and increased oval cell proliferation

MFGE-8 protein, contained in MSC-EXO cargo, improved liver phenotype *in vivo*

MEFG-8 expression was decreased in liver tissue biopsies from patients with AHF

EXO or rMFGE-8 administration rescued AHF by suppressing PI3K signaling
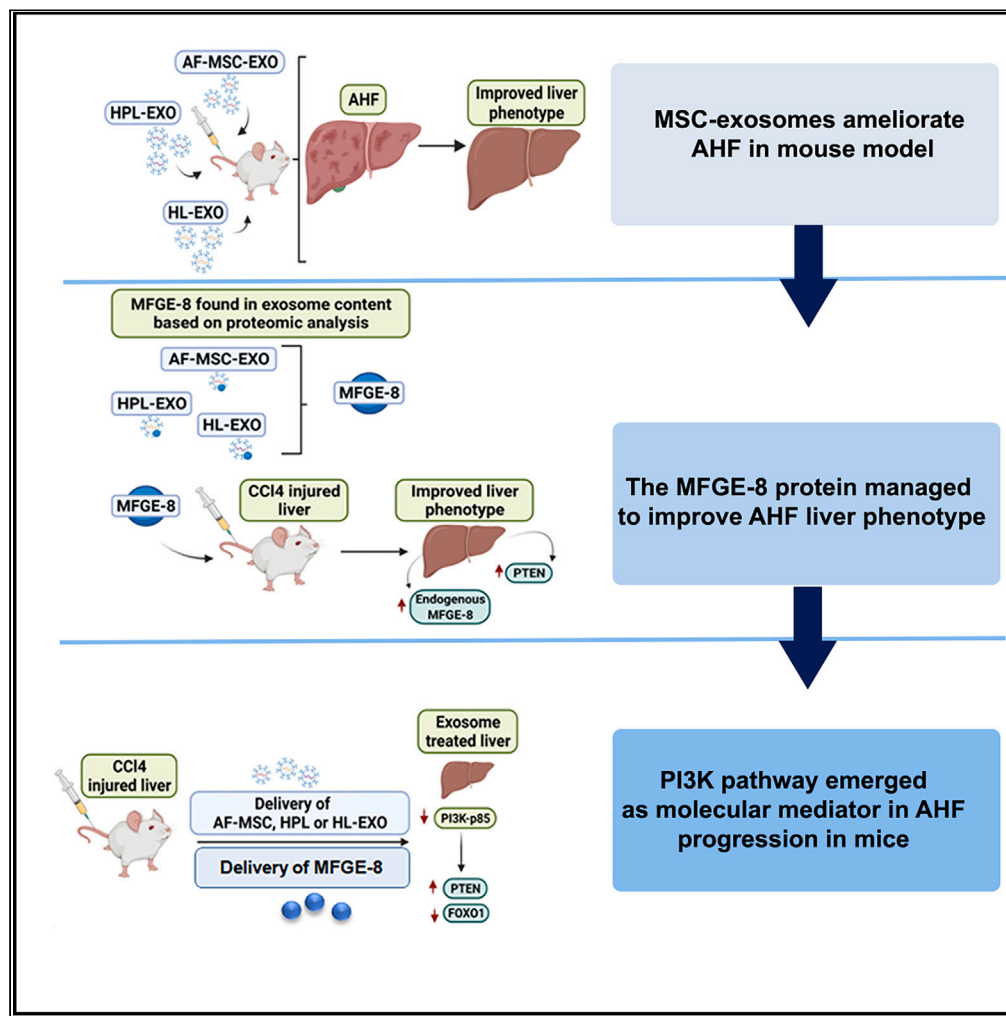
CellPress

Article

MFGE-8 identified in fetal mesenchymal-stromal-cell-derived exosomes ameliorates acute hepatic failure pathology

Adriana Psaraki,[1,2] Dimitra Zagoura,[1] Lydia Ntari,[1] Manousos Makridakis,[3] Christina Nikokiraki,[1,2] Ourania Trohatou,[1] Konstantina Georgila,[1] Christos Karakostas,[1] Ioanna Angelioudaki,[1] Anastasios G. Kriebardis,[4] Roberto Gramignioli,[5,6] Stratigoula Sakellariou,[7] Maria Xilouri,[8] Aristides G. Eliopoulos,[1] Antonia Vlahou,[3] and Maria G. Roubelakis[1,2,9,*]

SUMMARY

Liver transplantation is the gold-standard therapy for acute hepatic failure (AHF) with limitations related to organ shortage and life-long immunosuppressive therapy. Cell therapy emerges as a promising alternative to transplantation. We have previously shown that IL-10 and Annexin-A1 released by amniotic fluid human mesenchymal stromal cells (AF-MSCs) and their hepatocyte progenitor-like (HPL) or hepatocyte-like (HPL) cells induce liver repair and downregulate systemic inflammation in a CCl_4-AHF mouse model. Herein, we demonstrate that exosomes (EXO) derived from these cells improve liver phenotype in CCl_4-induced mice and promote oval cell proliferation. LC-MS/MS proteomic analysis identified MEFG-8 in EXO cargo that facilitates rescue of AHF by suppressing PI3K signaling. Administration of recombinant MFGE-8 protein also reduced liver damage in CCl_4-induced mice. Clinically, MEFG-8 expression was decreased in liver biopsies from AHF patients. Collectively, our study provides proof-of-concept for an innovative, cell-free, less immunogenic, and non-toxic alternative strategy for AHF.

INTRODUCTION

Acute hepatic failure (AHF) is a condition typified by rapid deterioration of hepatocellular function, including coagulopathy and hepatic encephalopathy.[1] The pathogenic background and the clinical etiologies of AHF are diverse.[2,3] In Western Europe, idiosyncratic drug reactions comprise the etiology of about 15% of AHF cases. Viral hepatitis is the predominant cause of AHF although acute viral hepatitis A and B cause AHF infrequently.[1,4,5] Recently, severe acute hepatitis of unknown origin, resulting in liver failure, was reported in children under the age of 10 years. Until now, 26 children required liver transplantation, whereas 10 died.[6] To date, liver replacement is the sole successful procedure for diseases causing cirrhosis and consecutively organ failure in end-stage disease.[7] Despite rescue potential, liver transplantation remains a non-specific approach that is limited by donor organ shortage and a life-long immunosuppressive therapy with related risks.[1,5]

Recently, cell-based therapies for AHF have been proposed with mesenchymal stromal cells (MSCs) as promising effectors.[7] MSC therapeutic applications in pre-clinical models of AHF offer hepatoprotection and suppression of the inflammatory process.[7–9] Similarly to solid organ transplantation, limitations in MSC therapies include donor unavailability exacerbated by high number of cells, cell heterogeneity, stability, differentiation capacity, immunocompatibility, and limited engraftment.[10] Interestingly, human fetal MSCs, such as amniotic fluid (AF) MSCs represent an advantageous cell type for allogeneic transplantation, because they exhibit inherently low immunogenic profile, higher proliferation rate, and differentiation potential compared with gold-standard adult bone marrow MSCs.[10–14]

However, implantation of intact donor cells is not always required; recent studies suggested hepatospecific MSC-based therapies could benefit liver diseases mainly due to a paracrine effect.[15] We have previously reported that interleukin (IL)-10 and Annexin-A1 (ANXA1) released by human AF-MSCs and hepatic progenitor-like (HPL) cells support liver regeneration in AHF induced by CCl_4 administration in NOD/SCID mice and reverse systemic inflammation.[14,16]

[1]Laboratory of Biology, School of Medicine, National and Kapodistrian University of Athens (NKUA), Athens, Greece
[2]Cell and Gene Therapy Laboratory, Centre of Basic Research, Biomedical Research Foundation of the Academy of Athens (BRFAA), Athens, Greece
[3]Biotechnology Laboratory, Centre of Basic Research, Biomedical Research Foundation of the Academy of Athens (BRFAA), Athens, Greece
[4]Laboratory of Reliability and Quality Control in Laboratory Hematology (HemQcR), Department of Biomedical Sciences, Section of Medical Laboratories, School of Health & Caring Sciences, University of West Attica (UniWA), Ag. Spyridonos Str, 12243 Egaleo, Greece
[5]Clinical Pathology and Cancer Diagnosis Unit, Karolinska Institute, 141 57 Huddinge, Sweden
[6]Experimental Cancer Medicine, Institution for Laboratory Medicine, Karolinska Institute, 171 77 Stockholm, Sweden
[7]First Department of Pathology, School of Medicine, National and Kapodistrian University of Athens (NKUA), Athens, Greece
[8]Center of Clinical Research, Experimental Surgery and Translational Research, Biomedical Research Foundation of the Academy of Athens (BRFAA), Athens, Greece
[9]Lead contact
*Correspondence: roubel@med.uoa.gr
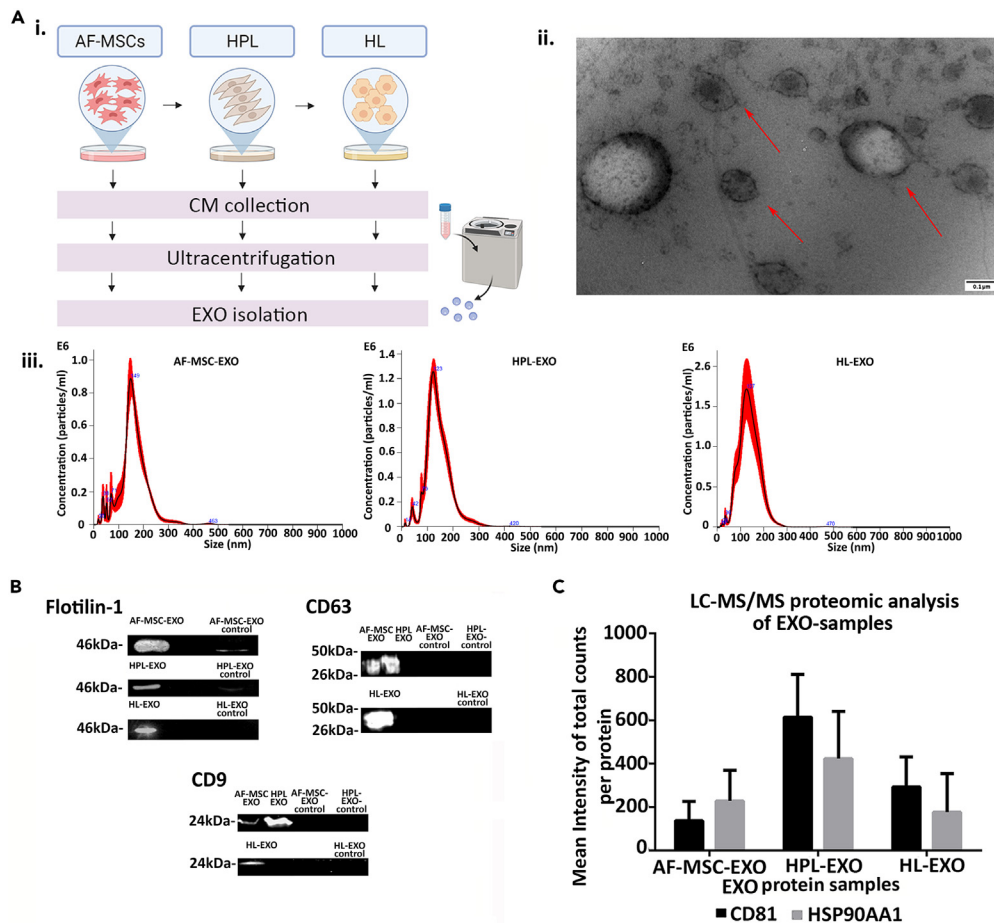https://doi.org/10.1016/j.isci.2023.108100

Figure 1. Characterization of AF-MSC-EXO, HPL-EXO, and HL-EXO

(A) (i) Schematic illustration of AF-MSC-EXO, HPL-EXO, and HL-EXO production (Created with Biorender.com). (ii) Representative TEM image of EXO (red arrows indicate EXO, magnification 29000×, scale bar: 0.1 μm). (iii) Evaluation of size distribution and concentration of exosomes using NTA analysis in AF-MSC-EXO-, HPL-EXO-, and HL-EXO-enriched samples.

(B) Representative WB figures (cropped) for exosomal marker expression.

(C) Bar chart depicts the levels of expression of CD81 and HSP90AA1 proteins measured by LC-MS/MS. Data represented as mean ± SEM (n = 6).

MSC mediators (collectively known as secretome) are released in high quantity as soluble proteins (chemokines or cytokines) but also embedded in extracellular vesicles (EVs) of micro- and nano-size (exosomes). Remarkably, MSC-derived exosomes (MSC-EXO) can deliver immunomodulatory and antiinflammatory molecules.[17,18] Several studies advocate the therapeutic potential of MSC-EVs in acute and chronic liver diseases and hepatocellular carcinoma (HCC).[18,19] Moreover, MSC-EXO exert a superior safety profile,[17,18,20] compared with intact cells they derive from, because they can be stored long-term without losing their properties,[21,22] do not generate thrombotic effects, and can be also engineered for drug therapy.[19,23]

Herein, we address an alternative concept in AHF therapy, whereby the infusion of MSC-EXO generated by human AF-MSCs (AF-MSC-EXO), hepatic progenitor-like cells (HPL-EXO), or hepatic-like cells (HL-EXO) ameliorates liver pathology and rescues CCl4-induced animals. We specifically explored the beneficial effects of AF-MSC-EXO, HPL-EXO, and HL-EXO *in vitro*, *ex vivo*, and *in vivo* using mouse models of AHF. We profiled the entire spectrum of AF-MSC-EXO, HPL-EXO, and HL-EXO protein cargoes and identified milk fat globule-EGF factor 8 (MFGE-8) as a key cargo responsible for AHF rescue. We further demonstrate that administration of recombinant MFGE-8 (rMFGE-8) recapitulates the protective effects of exosomes, underscoring promising perspectives in AHF therapy.

RESULTS

Characterization of AF-MSC-EXO, HPL-EXO, and HL-EXO by NTA, WB, and TEM analyses

AF-MSCs were cultured, characterized, and differentiated into HPL and HL cells, as described in supplemental information.[16,24–26] EXO were isolated from AF-MSC-CM, HPL-CM, or HL-CM through differential ultracentrifugation, as previously reported (Figure 1Ai). Their size ranged from 100 to 150 nm, as confirmed by TEM (Figure 1Aii). In addition, the average size (160.9 ± 2.0 nm, 143.3 ± 1.5 nm, 141 ± 3 nm), as well as

the average number of nanoparticles/mL PBS ($7.5 \times 10^7 \pm 2.30 \times 10^6$/mL, $1.05 \times 10^8 \pm 6.52 \times 10^6$/mL, $1.7 \times 10^8 \pm 3.57 \times 10^7$/mL) in AF-MSC-EXO-, HPL-EXO-, and HL-EXO-enriched samples, respectively, were also estimated by NTA (Figure 1Aiii). The isolated EXO were further validated for the expression of characteristic positive markers, including Flotillin-1, CD63 and CD9, and negative markers, such as GRP94 as determined by WB analysis[27] (Figures 1B and S1A, and Data S1), as well as CD81 and HSP90, as confirmed by proteomic analysis (Figure 1C).

Functional improvement of liver injury after EXO administration

Administration of CCl_4 induces inflammation, hepatocyte necrosis, oxidative stress, and extensive vacuolar degeneration in most parenchymal zones of the liver tissue, mimicking human AHF.[23] Liver damage was monitored by assessment of serum levels of aspartate transaminase (AST) and alanine transaminase (ALT) (Figure 2Bi). It was found that CCl_4 administration increased AST/ALT levels to 1511.89 ± 72.31 U/mL and 1399.56 ± 74.47 U/mL, respectively, compared with healthy mice (118.06 ± 10.07 U/mL and 71.33 ± 8.43U/mL), confirming liver injury (Figure 2Bii).

Ex vivo live imaging at 24 h after CCl_4 intoxication confirmed the hepatic delivery of PKH26-labeled EXO into CCl_4-induced $Rag^{-/-}$ mice, both after i.h. and i.v. administration (Figure 2Ai). The i.h. administration of PKH26-labeled EXO resulted in higher efficiency (8.53 ± 0.002 total counts/number of pixels) (Figure 2Aii) compared with the i.v. administration (8.05 ± 0.001 total counts/number of pixels) (Figure 2Aii). The co-localization of PKH26-labeled EXO and $CD24^+$ cells also confirmed the uptake of EXO into host hepatocytes after i.h. administration (Figure S1B).

On the basis of this observation, we proceeded with i.h. administration of EXO or CM into CCl_4-induced mice (Figure 2Bi). Twenty-four hours after the administration of AF-MSC-EXO, HPL-EXO, or HL-EXO, the AST levels were significantly decreased to 634.66 ± 138.53 U/mL, 443.75 ± 147.66 U/mL, and 515.4 ± 129.41 U/mL, respectively, and the ALT levels were reduced to 827.64 ± 155.8 U/mL, 356.25 ± 230.21 U/mL, and 362.3 ± 97.84 U/mL, respectively, compared with CCl_4-induced mice (**$p < 0.01$, ***$p < 0.001$, ****$p < 0.0001$; ANOVA test) (Figure 2Bii). In contrast, the administration of EXO-controls failed to exert a significant effect on serological transaminase levels (Figure 2Bii). Similar results were obtained following administration of AF-MSC-CM, HPL-CM, or HL-CM, where both AST and ALT levels were found significantly reduced (Figure 2Bii).

Histological analysis of liver sections from CCl_4-induced mice treated with AF-MSC-CM, HPL-CM, HL-CM- or AF-MSC-EXO, HPL-EXO, and HL-EXO confirmed the amelioration of liver injury. The AF-MSC-EXO, HPL-EXO, and HL-EXO therapeutic effect was further evaluated by the decreased levels of the pro-inflammatory cytokines IL-1 (1.48 ± 0.45, 1.12 ± 0.28, and 1.24 ± 0.26) (*$p < 0.05$; ANOVA), tumor necrosis factor alpha (TNF-α) (1.02 ± 0.23, 0.66 ± 0.48, and 0.73 ± 0.07) (****$p < 0.0001$; ANOVA), and inflammasome, NLRP3 (0.9 ± 0.18, 1.1 ± 0.33, and 0.93 ± 0.15) (*$p < 0.05$; ANOVA) in treated groups, compared with CCl_4-induced mice (2.33 ± 0.17, 1.21 ± 0.02, and 1.55 ± 0.06, respectively) at mRNA level (Figures S1Ci–S1Ciii), as well as by the presence of restricted necrotic areas in liver tissue sections (Figure 2C). Moreover, the number of apoptotic cells, as determined by TUNEL assay, was significantly reduced upon AF-MSC-EXO, HPL-EXO, or HL-EXO administration (8.68 ± 1.38, 3.58 ± 1.96, 5.21 ± 1.30 apoptotic cells, respectively) compared with CCl_4-induced mice (19.89 ± 5 apoptotic cells) (*$p < 0.05$, **$p < 0.01$; ANOVA; Figure 2Di). Similarly, the administration of AF-MSC-CM, HPL-CM, or HL-CM significantly improved the necrotic phenotype (11.74 ± 2.1, 3.07 ± 0.54, and 11.78 ± 1.95 apoptotic cells, respectively) compared with CCl_4-induced mice (Figure 2Di).

In addition, increased levels of the anti-apoptotic marker BCL-2 were detected after EXO (0.76 ± 0.07, 1.55 ± 0.25, 0.81 ± 0.12, respectively) or CM treatments (1.35 ± 0.17, 1.26 ± 0.24, 1.42 ± 0.19, respectively) (*$p < 0.05$, ****$p < 0.0001$; ANOVA test) compared with the control group (0.57 ± 0.04) as indicated in Figure 2Dii. Lower frequency of lipid deposition, as determined from the percentage (%) Oil Red O-stained area was observed after the administration of AF-MSC-EXO, HPL-EXO, or HL-EXO (0.20 ± 0.04, 0.04 ± 0.01, 0.08 ± 0.01, respectively) in comparison to liver tissue from CCl_4-induced mice (0.46 ± 0.08) (*$p < 0.05$, **$p < 0.01$; ANOVA test) (Figures 2C and 2Ei). Similar results were obtained upon i.h. injection of AF-MSC-CM, HPL-CM, or HL-CM (Figures 2C and 2Ei). The decrease in lipid deposition was also indicated by a significant decrease in the hepatic RNA levels of PPARG upon EXO (0.72 ± 0.23, 0.47 ± 0.26, and 0.75 ± 0.22) or CM (0.78 ± 0.15, 1.23 ± 0.34, and 1.22 ± 0.21) delivery compared with control CCl_4-induced mice (1.61 ± 0.19, *$p < 0.05$; ANOVA test) (Figure 2Eii).

To determine whether the aforementioned effects may also occur in the presence of intact immune system, we injected AF-MSC-EXO in BALB/c mice 24 h after CCl_4 administration. We measured a significant decrease in AST (1956.67 ± 202.7; *$p < 0.05$; ANOVA test) and ALT (2074 ± 144.96) levels compared with CCl_4-induced animals in the absence of EXO (2393.25 ± 57.15093 and 2488.75 ± 137.62, respectively) (Figure S2Ai) and a lower frequency of necrotic areas (Figure S2Aii).

EXO confer proliferative effect on hepatic progenitors *ex vivo*

As we previously reported,[14,16] murine hepatic progenitors ($CD24^+$/$Ter119^-$) are mobilized after acute liver injury to repair tissue damage.[18,19] To examine whether exosomes can also promote oval cell proliferation, we exposed $CD24^+$/$Ter119^-$ murine hepatic progenitors harvested from CCl_4-induced mice, to media containing EXO. We observed different levels of enhanced oval cell proliferation when exposed to AF-MSC-EXO (35.47 ± 12.21%, *$p < 0.05$; ANOVA test), HPL-EXO (9.74 ± 3.78%, *$p < 0.05$; ANOVA test), or HL-EXO (9.98 ± 3.58%, *$p < 0.05$; ANOVA test) compared with exosome-negative controls (Figure 2F). Exposure of hepatic progenitors to AF-MSC-CM, HPL-CM, and HL-CM also resulted in high proliferation rates of oval cells (26.65 ± 4.59%, 30.72 ± 10.09%, and 11.87 ± 5.40%, respectively) (Figure 2F).

Proteomic analysis of EXO cargoes identifies proteins and pathways with antiinflammatory and regenerative potential

To identify components of exosomes that mediate therapeutic effects on AHF, we analyzed the protein content of AF-MSC-EXO, HPL-EXO, and HL-EXO using high-resolution LC-MS/MS (Figure 3A). A total of 253 peptides were identified from all categories, each represented by 6
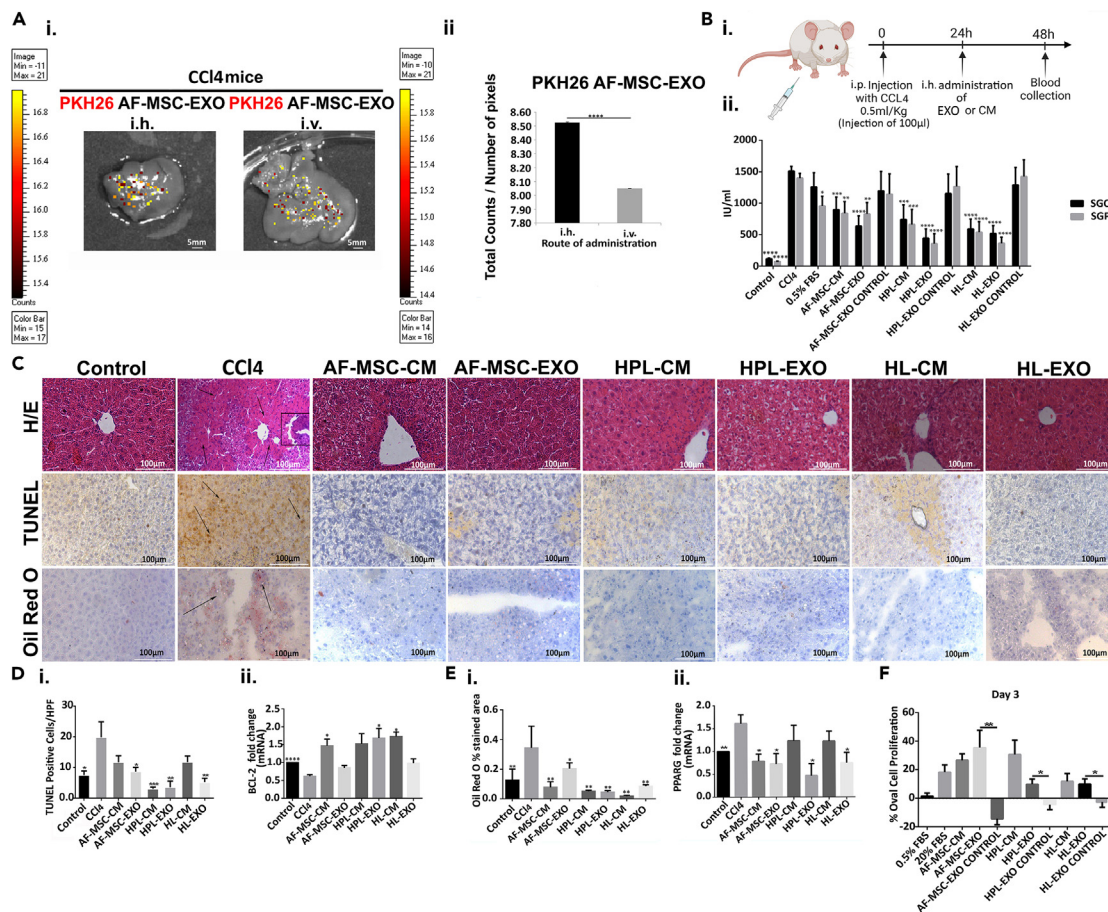
Figure 2. Investigation of the therapeutic effect of AF-MSC-EXO, HPL-EXO, or HL-EXO in CC₄-mice

(A) (i) Representative IF image of AF-MSC-EXO labeled with PKH26 and delivered i.h. or i.v. to CCl₄-induced mice. (ii) Quantification of PKH26 labeled AF-MSC-EXO after i.h. and i.v. administration (****p < 0.0001; ANOVA test). Scale bar: 5 mm.

(B) (i) Schematic overview of CCl₄ induction and treatment of Rag⁻/⁻ mice (Created with Biorender.com). (ii) Levels of serological AST and ALT transaminases after CCl₄ injection and administration of AF-MSC-EXO, HPL-EXO, HL-EXO (n = 10 animals/group, **p < 0.01, ****p < 0.0001; ANOVA test), or AF-MSC-EXO control, HPL-EXO control, HL-EXO control (n = 10 animals/group), or AF-MSC-CM, HPL-CM, HL-CM (n = 10 animals/group, **p < 0.01,***p < 0.001, ****p < 0.0001; ANOVA test) or 0.5% FBS medium, (n = 10 per group, *p < 0.05; ANOVA test). Data are represented as mean ± SEM (n = 10/group). P-values were estimated versus CCl₄-induced mice group.

(C) Representative images of H&E, Oil Red O, and TUNEL stainings in liver tissue from EXO- or CM-treated CCl₄-induced mice. Areas of necrosis and inflammation, TUNEL positive cells, or red droplets are indicated (black arrows). Original magnification 20×. Scale bar: 100 μm.

(D) (i) Bar chart depicts the mean number of apoptotic cells after respective treatments (n = 3 mice/group, *p < 0.05, **p < 0.01; ***p < 0.001 ANOVA test). Data are represented as mean ± SEM positive cells (n = 20 randomly selected fields). (ii) Bar chart of BCL-2 mRNA levels after treatments compared with CCl₄-induced mice (n = 3/group, *p < 0.05, ****p < 0.0001; ANOVA test). Gene expression levels were normalized to GAPDH.

(E) (i) Bar chart represents the percentage of Oil-Red-O-stained area after treatments (n = 3/group, *p < 0.05, **p < 0.01; ANOVA test). Data represented as mean ± SEM positive cells (n = 20 randomly selected fields). (ii) Bar chart depicts the PPARG mRNA expression in treated groups (n = 3/group, *p < 0.05, **p < 0.01; ANOVA test). Gene expression levels were normalized to GAPDH.

(F) Bar chart depicts the proliferation rates of oval cells treated with AF-MSC-, HPL-, and HL-secreted mediators. DMEM (20% FBS) (positive control), DMEM (0.5% FBS) (negative control), and AF-MSC-EXO, HPL-EXO, and HL-EXO controls were used. Data are represented as mean ± SEM (n = 3) (*p < 0.05, **p < 0.01; ANOVA test).

biological replicates. When compared with the top100 exosomal proteins listed in ExoCarta (http://www.exocarta.org) and Vesiclepedia (http://microvesicles.org/) databases, the EXO components overlapped by 50% with ExoCarta and 44% with Vesiclepedia, representing a total of 39 proteins in common (Figures 3Bi and 3Ciii). In order to elucidate protein similarities among the 6 EXO replicates from each category, principal component analysis (PCA) was performed. The HPL-EXO and HL-EXO groups were clustered together, whereas the AF-MSC-EXO group exhibited higher variability levels (Figure 3Bii).

Comparison of the contents of EXO categories identified a group of 30 proteins that are represented in all group samples (Figures 3Ci and 3iii, and Table S3) and are thus putative mediators of the therapeutic effect of AF-MSC, HPL, and HL exosomes. Subsequently, 3 levels of
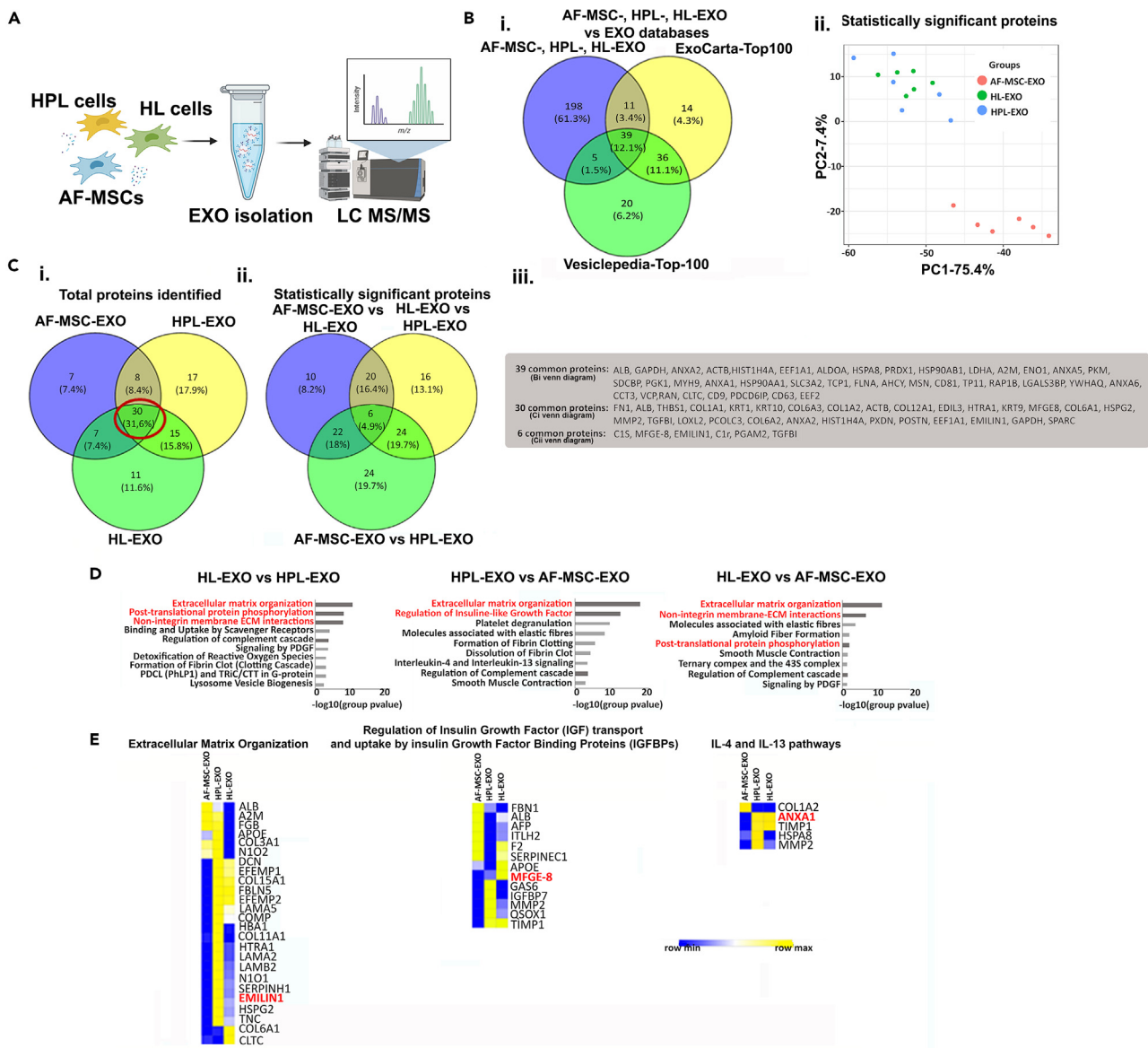
Figure 3. Proteomic and bioinformatics analysis of AF-MSC-EXO, HPL-EXO, and HL-EXO samples

(A) Schematic presentation of the EXO proteomic analysis (Created with Biorender.com).

(B) (i) Venn diagram showing the overlapping proteins from AF-MSC-EXO, HPL-EXO, and HL-EXO data versus data from ExoCarta and Vesiclepedia databases (n = 6). (ii) PCA plot depicting the 6 common proteins present in AF-MSC-EXO, HPL-EXO, and HL-EXO samples.

(C) (i) Venn diagram depicts the number of common and unique proteins between AF-MSC-EXO, HPL-EXO, and HL-EXO samples (n = 6). (ii) Venn diagram represents the number of the statistically significant common and unique proteins identified from the comparisons: AF-MSC-EXO versus HL-EXO, HL-EXO versus HPL-EXO, and AF-MSC-EXO versus HPL-EXO. (iii) Table summarizing the common proteins between EXO data and EXO databases.

(D) Bar charts showing the statistically significant pathways retrieved from AF-MSC-EXO versus HL-EXO, HL-EXO versus HPL-EXO, and AF-MSC-EXO versus HPL-EXO comparisons. Red color stands for the most represented and common pathways among the comparisons.

(E) Heatmaps illustrate selected statistically significant proteins clustered in 3 signaling pathways and presented as differentially expressed among AF-MSC-EXO, HPL-EXO, or HL-EXO samples. Blue color indicates downregulation, yellow color indicates upregulation of the selected proteins, and red color indicates the 2 out of the 6 statistically significant and common proteins among all EXO comparisons (EMILIN-1 and MFGE-8) and ANXA1 molecule.

comparisons were made: AF-MSC-EXO versus HL-EXO, HPL-EXO versus HL-EXO, and AF-MSC-EXO versus HPL-EXO (Figure S3 and Table S4). As shown in the Venn diagram of Figure 3Cii, the overlap of these comparisons is represented by 6 proteins: C1s, C1r, EMILIN-1, MFGE-8, PGAM2, and TGFB1 (Figure 3Ciii). Conversely, 7 proteins were uniquely identified in AF-MSC-EXO samples, 17 in HPL-EXO samples, and 11 in HL-EXO samples (Figure 3Ci, Tables S1 and S4).
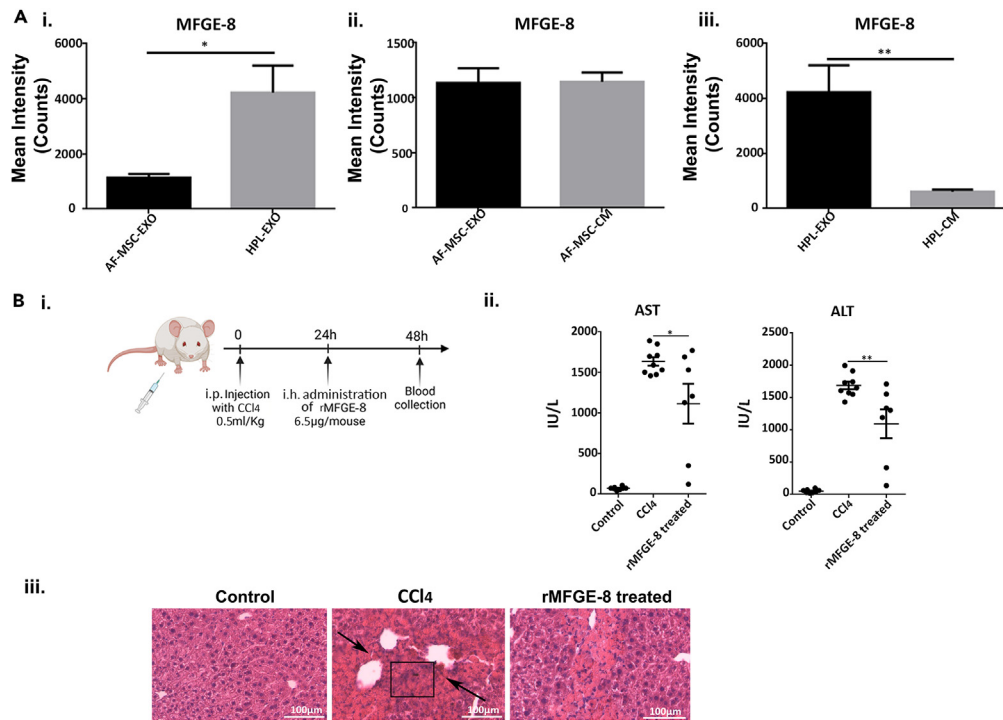
Figure 4. Comparison of the expression levels of MFGE-8 in AF-MSC-EXO and HPL-EXO cargoes with AF-MSC-CM and HPL-CM and investigation of its therapeutic effect on CCl$_4$-induced mice

(A) (i) Quantification of the mean intensity of MFGE-8 protein in AF-MSC-EXO and HPL-EXO samples. Data represented as mean ± SEM (n = 6) (*p < 0.05; Mann-Whitney test). Bar chart represents the comparison of mean intensity levels of MFGE-8 between (ii) AF-MSC-EXO versus AF-MSC-CM; data represented as mean ± SEM (n = 4) (p > 0.05; Mann-Whitney test) and (iii) HPL-EXO versus HPL-CM samples; data represented as mean ± SEM (n = 4) (**p < 0.001; Mann-Whitney test).

(B) (i) Schematic presentation of CCl$_4$ induction of AHF in mice and subsequent treatment with rMFGE-8. Biochemical analysis was conducted in blood sera 24 h after the treatment (Created with Biorender.com). (ii) Dot plot depicts levels of AST and ALT in CCl$_4$-induced mice treated with rMFGE-8. Data represented as mean ± SEM (n = 7) (*p < 0.05, **p < 0.01; ANOVA test). (iii) Histological analysis of liver sections after the administration of rMFGE-8 in CCl$_4$-induced mice. Black arrows indicate the necrotic areas. Original magnification 20×. Scale bar: 100 μm.

Further bioinformatics analysis of each EXO comparison indicated 3 pathways as the most common and highly represented: (1) extracellular matrix (ECM) organization, (2) non-integrin membrane-ECM interactions, and (3) post-translation protein phosphorylation (Figure 3D and Table S4). EMILIN-1 clustered in ECM organization, MFGE-8 in posttranslation protein phosphorylation pathway, and C1s and C1R in the regulation of complement cascade (Figure 3D and Table S4).

An extended *in silico* analysis of identified proteins (Table S4) was performed in relation to wound healing and liver regeneration and showed them to cluster in 3 signaling pathway groups: (1) the ECM organization pathway, (2) regulation of insulin growth factor (IGF) transport and uptake by insulin growth factor binding proteins (IGFBPs) pathway, and (3) IL-4 and IL-13 pathway (Figure 3E). EMILIN-1 and MFGE-8 were listed in ECM organization and IGF transport and uptake by IGFBPs pathways, respectively (Figure 3E). Interestingly, ANXA1 molecule, whose therapeutic effect was previously investigated in AHF mouse model,[14] was listed in IL-4 and IL-13 pathway (Figure 3E).

MFGE-8 mediates the therapeutic effects of EXO on AHF

We have previously shown that ANXA-1 released by human AF-MSCs and HPL cells confers antiinflammatory effects in the CCl$_4$ mouse model of AHF.[14] ANXA-1 has also been reported to increase dendritic cell efferocytosis and antigen presentation.[28] Similar to ANXA1, MFGE-8 is involved in efferocytosis[29] and has been suggested as potential therapeutic target for the treatment of liver steatosis and fibrosis.[30,31] Consequently, we focused our attention to MFGE-8 in relation with AHF pathogenesis.

Previous studies support the superior role of AF-MSCs and HPL cells compared with HL cells,[16] as well as the therapeutic effect of HPL-CM in mice with CCl$_4$-induced liver injury.[14,16] Interestingly, we measured by LC-MS/MS analysis higher level of MFGE-8 in HPL-EXO (4222.9 ± 984.7 peaks) compared with AF-MSC-EXO (1135.9 ± 132.4 peaks) (*p < 0.005; Mann-Whitney test) (Figures 4Ai and S4A, and Table S4, Data S1). We completed our analysis by comparing the proteomic profiles of AF-MSC-EXO and HPL-EXO with the ones of AF-MSC-CM and HPL-CM.[16] The levels of protein expression in AF-MSC versus HPL secreted mediators (CM and EXO), revealed 110 proteins (18.2%) in common, including MFGE-8 (Figures S4B, S4Ci, and S4Cii, Tables S2 and S5). When AF-MSC-EXO were compared with AF-MSC-CM, no significant difference in MFGE-8 levels was found (1135.9 ± 132.4 for EXO and 1144.4 ± 83.5 for CM, respectively) (Figures 4Aii and Table S5); however,
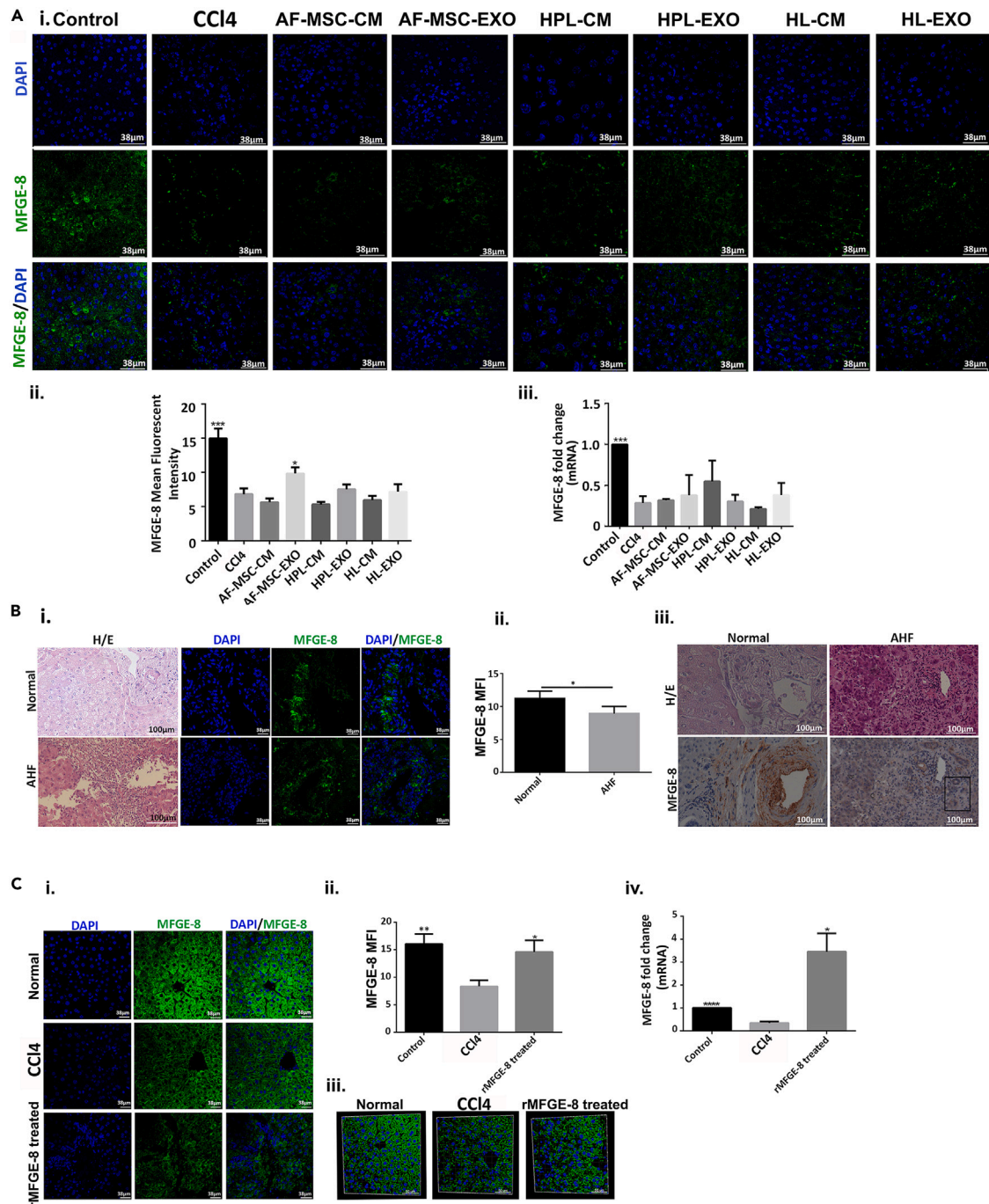
Figure 5. Analysis of the expression levels of endogenous MFGE-8 in liver tissue from CCl₄-induced mice treated with AF-MSC-EXO, HPL-EXO, HL-EXO or rMFGE-8 and in liver biopsies from patients with AHF

(A) Analysis of endogenous levels of MFGE-8 protein in liver of treated CCl₄-induced mice. (i) Representative IF imaging of MFGE-8 (green) in liver tissue sections from CCl₄-mice, as well as from AF-MSC-EXO-, HPL-EXO-, or HL-EXO-treated CCl₄-mice. Nuclei are shown in blue. Original magnification 63×. Scale bar: 38 μm. (ii) Bar chart represents the MFI in liver sections of treated CCl₄-mice compared with positive control. Data are represented as mean $\pm$ SEM from at least 20 randomly selected fields (n = 3 animals/group, *p < 0.05, ***p < 0.001, ANOVA test). (iii) Bar chart depicts the fold change of mRNA levels of MFGE-8 in normal mice (***p < 0.001, ANOVA test) and treated CCl₄-mice. Data are represented as mean $\pm$ SEM (n = 3/group; ANOVA test) compared with CCl₄-mice. (B) Analysis of MFGE-8 expression levels in biopsies from AHF patients. (i) Representative IF images of normal and AHF patients' biopsies. Original magnification ×68. Scale bars: 100 μm and 38 μm, respectively. (ii) Bar chart depicts the MFI of MFGE-8 expression. Data are represented as means $\pm$ SEM from randomly

selected fields (n = 10/slide, *p < 0.05; ANOVA test). (iii) Representative immunohistochemical images showing the MFGE-8 expression in normal samples and samples from AHF patients. Original magnification 20×. Scale bar: 100 μm.
(C) Analysis of the endogenous levels of MFGE-8 in liver of CCl_4-induced mice treated with rMFGE-8. (i) Representative IF images of MFGE-8 expression (green) in liver sections from normal, CCl_4-induced mice, and CCl_4-induced mice posttreatment with rMFGE-8. Nuclei are shown in blue. Original magnification 63×. Scale bar: 38 μm. (ii) Bar chart depicts the MFI in liver sections of normal mice, CCl_4-induced mice, and CCl_4-induced mice treated with rMFGE-8. Data are represented as means ± SEM from at least 20 randomly selected fields (n = 3 animals/group, *p < 0.05, **p < 0.01; ANOVA test). (iii) Imaris illustration of 3D expression of MFGE-8 in normal mice, CCl_4-induced mice, and CCl_4-induced mice treated with rMFGE-8. Original magnification 68×. Scale bar: 50 μm. (iv) Bar chart represents the mRNA expression levels of MFGE-8 in normal mice and CCl_4-induced mice treated with rMFGE-8 compared with positive control. Data are represented as means ± SEM (n = 3 per group, ****p < 0.0001, *p < 0.05; ANOVA test). Gene expression levels were normalized to GAPDH.

the levels of MFGE-8 were significantly higher (**p < 0.001; Mann-Whitney test) in HPL-EXO (4222.9 ± 984.7) compared with HPL-CM (614.3 ± 74.7) (Figures 4Aiii and Table S5).

To directly link MFGE-8 with improved AHF outcomes, we administered recombinant MFGE-8 (rMFGE-8) to CCl_4-induced $Rag^{-/-}$ mice (Figure 4Bi). We observed reduction in the levels of ALT and AST (1113.86 ± 244.75 U/mL, *p < 0.05 and 1091.29 ± 223.03 U/mL, **p < 0.01) compared with the control CCl_4-induced group (1633.78 ± 57.04 U/mL and 1687.78 ± 59.67 U/mL, respectively, ****p < 0.0001; ANOVA test) (Figure 4Bii), as well as reduced necrotic areas and inflammatory cell infiltration (Figure 4Biii). We conclude that MFGE-8 alleviates liver pathology in AHF.

Expression of MFGE-8 is reduced in the liver of AHF patients and the CCl_4 mouse model of AHF

On the basis of the aforementioned observations, we hypothesized that MFGE-8 may be differentially expressed in AHF. By immunofluorescence, we found that the hepatic levels of MFGE-8 in CCl_4-induced animals are reduced (mean fluorescent intensity [MFI] = 6.86 ± 0.84) compared with healthy controls (MFI = 14.08 ± 1.3; ****p < 0.0001, ANOVA test) (Figures 5Ai and 5Aii). We also used IF to analyze MFGE-8 expression in liver biopsies from healthy individuals and AHF patients. AHF biopsies exhibited confluent bridging, panlobular or submassive hepatocellular necrosis, and lower levels of MFGE-8 (7.86 ± 2.27) compared with healthy liver (12.14 ± 1.12, *p < 0.05; ANOVA test) (Figures 5Bi and 5Bii). Histologically, hepatic expression of MFGE-8 was predominantly detected on the edge of portal vein in healthy subjects, but around bile ducts and some endothelial cells in AHF patients (Figure 5Biii).

Next, we examined whether EXO administration may impact the expression of MFGE-8 in the liver of CCl_4-induced mice. By immunofluorescence analysis, we found that the hepatic levels of MFGE-8 in these animals are reduced (MFI = 6.86 ± 0.84) compared with healthy controls (MFI = 14.08 ± 1.3; ****p < 0.0001, ANOVA test) (Figures 5Ai and 5Aii). Importantly, i.h. administration of EXOs from AF-MSC, HPL, or HL partially restored the expression of MFGE-8 in the liver of CCl_4-induced mice (9.85 ± 0.88, 7.54 ± 0.7, and 7.17 ± 1.12, respectively, *p < 0.05; ANOVA test) (Figures 5Ai and 5Aii). The increase in MFGE-8 protein levels likely reflects changes in *MFGE-8* transcription as mice administered AF-MSC-EXO, HL-EXO, or HPL-CM expressed higher MFGE-8 mRNA levels (0.38 ± 0.25; 0.38 ± 0.15; 0.55 ± 0.25, respectively) compared with CCl_4-induced mice (0.28 ± 0.08) (Figure 5Aiii).

Furthermore, immunofluorescence analysis on CCL_4-induced mice treated with rMFGE-8 revealed increased levels of MFGE-8 expression (14.58 ± 2.13, *p < 0.05; ANOVA test) compared with untreated CCl_4-induced mice (8.95 ± 1.15) (Figures 5Ci and 5Cii). Three-dimensional analysis of murine parenchyma, by Imaris software, revealed a peculiar MFGE-8 distribution, with accumulation around liver vessels, in rMFGE-8-treated mice (Figure 5Ciii). Similarly, transcriptome analysis revealed increased MFGE-8 levels (3.45 ± 0.80, *p < 0.05; ANOVA test) compared with CCl_4-induced mice (0.34 ± 0.07) (Figure 5Civ).

MFGE-8 regulates the PI3 kinase pathway in the liver

To obtain indications of the mechanism by which MFGE-8 mediates the therapeutic effects of EXO on AHF, we explored FLAME (https://bib.fleming.gr:8084/app/flame),[32] a web tool for functional and literature enrichment analysis of multiple datasets. Specifically, we used FLAME to analyze the 30 proteins comprising the intersection of all EXO groups (Figure 6Ai) and the proteins identified by the proteomic comparison of secreted mediators of AF-MSC versus HPL (Figure 6Aii). Based on the Kyoto Encyclopedia of Genes and Genomes (KEGG), both sets were found enriched for the PI3K-Akt pathway with enrichment scores of 2% and 4.25%, respectively (Figures 6Ai and 6Aii). Further analysis using STRING uncovered a network of interacting molecules that include modulators of inflammation (IL-6, CD68), apoptosis (BCL-2), and regeneration (mTOR, AKT, STAT3) and suggested a potential link between MFGE-8 and the PI3K-Akt pathway (Figure 6Aiii). Prompted by these *in silico* predictions, we analyzed the effects of i.h. administration of EXO on the PI3K/AKT pathway in CCl_4-induced mice.

By RT-qPCR we quantified the mRNA levels of *PTEN*, a negative regulator of PI3K activity, and of the PI3K catalytic subunit p85. The results showed that administration of HPL-EXO (1.49 ± 0.41, *p < 0.05; ANOVA test) or HL-EXO (1.1 ± 0.07, *p < 0.05; ANOVA test) led to higher expression of PTEN compared with mice exposed to CCl_4 alone (0.61 ± 0.12) (Figure 6Bi). Increased expression of *PTEN* was also observed after AF-MSC-CM (1.7 ± 0.53, *p < 0.05; ANOVA test), HPL-CM (1.64 ± 0.3, *p < 0.05; ANOVA test), or HL-CM (1.41 ± 0.22, *p < 0.05; ANOVA test) administration (Figure 6Bi). In contrast, treatment with AF-MSC-EXO (0.85 ± 0.24), HPL-EXO (0.74 ± 0.2, *p < 0.05; ANOVA test), or HL-EXO (0.55 ± 0.11, **p < 0.01; ANOVA test) reduced the mRNA levels of *PI3K-p85* compared with the control CCl_4 group that did not receive EXO (1.55 ± 0.33) (Figure 6Bii). Similar results were obtained following administration of AF-MSC-CM, (90.79 ± 0.19, *p < 0.05; ANOVA test), HPL-CM (1.05 ± 0.3), or HL-CM (0.7 ± 0.13, *p < 0.05; ANOVA test) (Figure 6Bii).
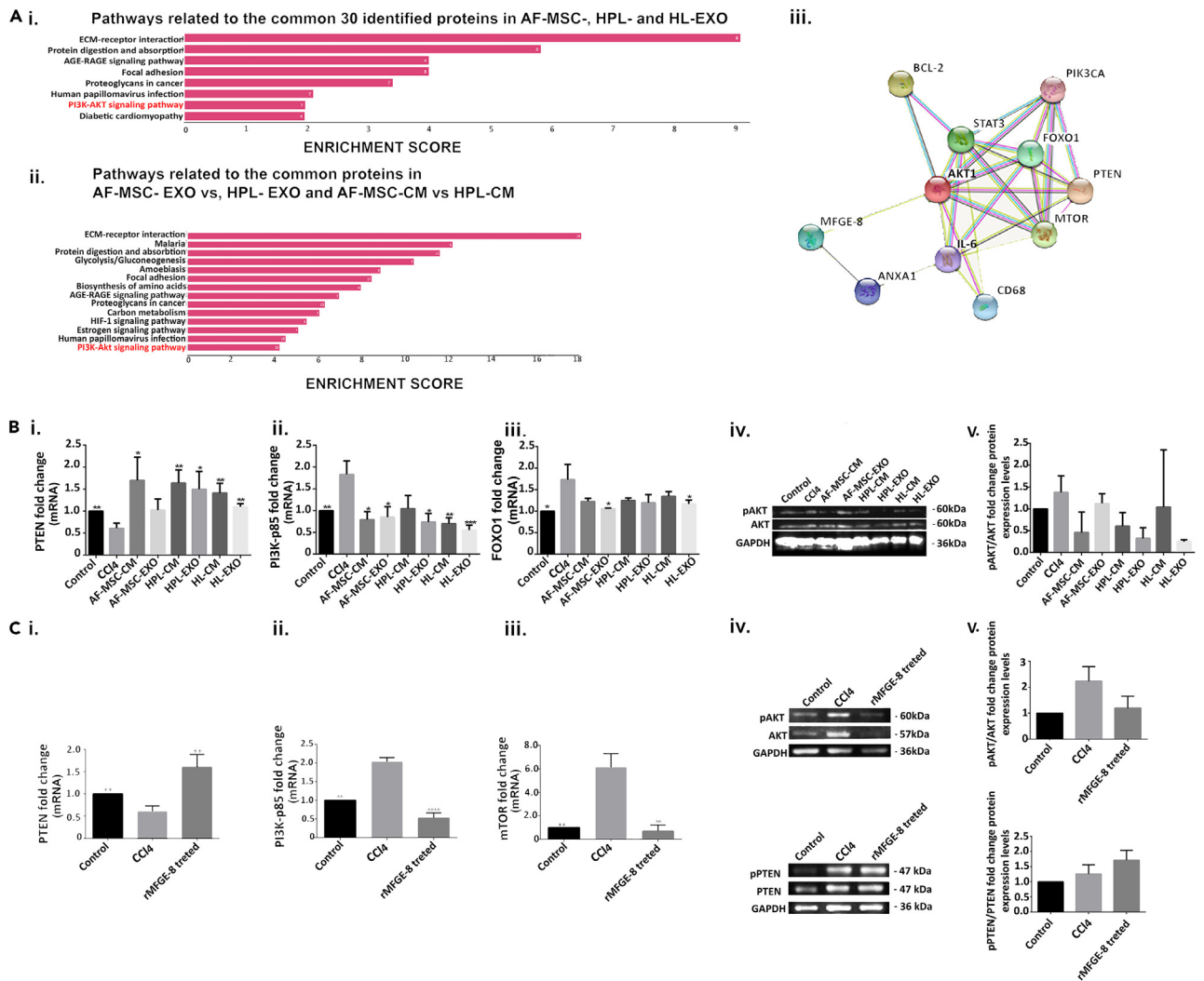
Figure 6. The activation of PI3K signaling pathway was determinant for the progression of AHF in CCl4-induced mice treated with EXO or rMFGE-8

(A) Analysis of the common proteins between EXO and CM groups using the FLAME software related to the (i) 30 common proteins identified in AF-MSC-EXO, HPL-EXO, HL-EXO samples and (ii) 110 common proteins identified in AF-MSC-CM, HPL-EXO-CM and HL-CM in terms of KEGG ontology. (iii) Schematic presentation of predictive network of MFGE-8 interactions with AKT1, PI3KCA, PTEN, FOXO1, MTOR, STAT3, CD68, ANXA1, BCL-2, and IL-6 using STRING. Black line indicates potential co-expression and yellow line text-mining interaction.

(B) Bar charts depict the fold-change mRNA levels of: (i) PTEN (n = 3/group, *p < 0.05, **p < 0.01; ANOVA test), (ii) PI3K-p85 (n = 3/group, *p < 0.05, **p < 0.01, ***p < 0.001; ANOVA test), and (iii) FOXO1 (n = 3/group, *p < 0.05; ANOVA test) in AF-MSC-EXO-, HPL-EXO-, or HL-EXO- treated CCl4-induced mice compared with CCl4-induced mice. Data represented as mean ± SEM. Gene expression levels were normalized to GAPDH. (iv) Representative WB image (cropped) for pAKT and AKT expression in liver tissue from treated CCl4-induced mice. (v) Bar chart depicts the pAKT/AKT ratio in liver tissue from CCl4 mice treated with AF-MSC-EXO, HPL-EXO, HL-CM, or HL-EXO. Data represented as mean ± SEM. GAPDH served as an internal control. (v) Bar chart depicts the pAKT/AKT fold changes in liver tissue from CCl4 mice treated with AF-MSC-CM, HPL-CM, HL-CM or AF-MSC-EXO, HPL-EXO, HL-EXO. GAPDH served as an internal control (n = 3, p = 0.0852, p = 0.2057, p = 0.3613, and p = 0.1534, p = 0.0719, and p = 0.0629, respectively; ANOVA test).

(C) Bar charts depict the mRNA expression levels for (i) PTEN (n = 3/group, **p < 0.01; ANOVA test), (ii) PI3K-p85 (n = 3/group, **p < 0.01, ****p < 0.0001; ANOVA test), and (iii) mTOR (n = 3/group, **p < 0.01; ANOAVA test) in rMFGE-8-treated mice, compared with untreated CCl4-induced mice. Data represented as mean ± SEM. (iv) Representative western blot image (cropped) of analysis of pAKT, AKT, and PTEN and pPTEN expression protein levels in rMFGE-8-treated mice compared with untreated CCl4-induced mice. (v) Bar charts depict the pAKT/AKT and pPTEN/PTEN fold changes of protein expression levels in rMFGE-8-treated mice compared with untreated CCl4-induced mice. GAPDH was served as an internal control mice (n = 3, p = 0.2257, and p = 0.4016, respectively, ANOVA test). Data represented as mean ± SEM.

Immunoblot analysis of liver lysates for the phosphorylated AKT (pAKT), a surrogate for PI3K activation, indicated a downregulation trend of PI3K signaling pathway in AF-MSC-, HPL-, and HL-derived EXO treatment groups (Figure 6Biv) (pAKT/AKT fold changes [1.12 ± 0.22, 0.32 ± 0.24 and 0.25 ± 0.04, respectively]) compared with CCl4-induced mice group (1.38 ± 0.38) (Figure 6Bv and Data S1).

Similar results were obtained following i.h. administration of AF-MSC-CM, HPL-CM, or HL-CM to CCl₄-induced mice compared with the control group that did not receive CM (Figure 6Biv). In line with the reduced levels of pAKT, the expression levels of *FOXO1*, which is mediated by activated AKT, was reduced upon i.h. administration of AF-MSC-EXO (1.06 ± 0.01), HPL-EXO (1.19 ± 0.19), HL-EXO (1.17 ± 0.09), AF-MSC-CM (1.23 ± 0.07), HPL-CM (1.25 ± 0.06), or HL-CM (1.34 ± 0.11) to CCl₄-induced mice compared with the control group that did not receive EXO or CM (1.73 ± 0.35) (Figure 6Biii).

To directly link MFGE-8 to the PI3K/AKT pathway, we assessed the mRNA levels of *PTEN* and *PI3K-p85* and the protein levels of pAKT in the liver of CCl₄-induced mice following i.h. administration of rMFGE-8 (Figure 6C). Similar to AF-MSC-EXO, HPL-EXO, and HL-EXO treatments, we observed significantly higher levels of *PTEN* mRNA levels in the liver of mice treated with rMFGE-8 (1.6 ± 0.28) compared with the control group that only received CCl₄ (0.61 ± 0.12, **$p < 0.01$; ANOVA test) (Figure 6Ci). In contrast, the expression levels of *PI3K-p85* and *mTOR* decreased (0.53 ± 0.13, ****$p < 0.0001$; ANOVA test and 0.71 ± 0.51, **$p < 0.01$; ANOVA test, respectively) upon rMFGE-8 treatment compared with CCl₄-controls (2.04 ± 0.10 and 6.14 ± 1.16, respectively) (Figures 6Cii and 6Ciii). In addition, the ratio pAKT/AKT decreased (1.2 ± 0.46), whereas pPTEN/PTEN increased (1.71 ± 0.33) in rMFGE-8-treated mice compared with CCl₄-induced mice (1.95 ± 0.34 and 1.25 ± 0.31, respectively), further indicating a downregulation trend of the PI3K/AKT signaling pathway by MFGE-8 (Figures 6Civ and 6Cv, and Data S1).

DISCUSSION

Accumulating evidence supports the therapeutic potential of MSC-derived soluble factors in several pathological conditions.[33] The MSC secretome is a multifactorial biological source of various cytokines, chemokines, and growth factors, released in soluble form or embedded into EVs.[19,34,35] Recent studies have demonstrated that MSC secretome may present considerable advantages over intact cell-based applications with respect to immunogenicity, manufacturing, storage with nontoxic cryopreservation as well as manipulation for safety and dosage as common pharmaceutical agent. Our previous studies uncovered secreted factors such as IL-10 and ANXA1 as effectors of fetal MSCs and underscored the potential of cell-free therapeutic modalities in liver regeneration.[14,16] Recently, several studies described massive release of EVs, such as exosomes, by different MSC sources[19,36,37] and showed the therapeutic potential of MSC-EXO in liver diseases, including liver fibrosis, cirrhosis, and HCC.[19] However, the specific factors embedded to and delivered by MSC-EXO and their mechanisms of action in relation to hepatoprotection remain largely unexplored.

Although there are several advantages by using either CM or EXO in the treatment of different diseases, including safety and handling, EV preparations exert some highly promising characteristics for clinical applications. In more detail, the preparation of CM may be a simple method but the limitations related to characterization and standardization of its components need to be addressed for clinically acceptable products, because until today the characterization of CM preparations is mainly based on the presence of pro-inflammatory factors. However, EV preparations can be easily characterized by their size, total protein concentration, number of particles, and specific surface markers.[19,38] EVs are also abundant in small RNAs, especially in miRNAs that play a crucial role in inflammation response and cancer resistance by targeting different cell types.[39] Moreover, it has been reported that exosomal small RNAs and miRNAs are protected against RNaseA, compared with cell-free circulating RNAs.[40] Alongside, the most advantageous characteristic of EVs for future advanced therapeutic treatments is their capability of modification to the desired loaded cargo or to target the desired target cell. The pharmaceutical agents can generally be encapsulated into purified EVs by methods such as incubation, sonication, and electroporation or EVs can be modified in order to be enriched for a specific protein or small RNA by respective treatment of parental cells. These loading mechanisms represent a preferable mechanism for therapeutic approach than CM or intact donor cell administration.[41,42] In addition, EVs are amenable to cell membrane modifications through membrane proteins (i.e., Lamp2B, GPI) for imaging, tracking, and cell-type-specific targeting, enhancing their targeting efficiency in site of injury and their therapeutic outcome as treatment or biomarker in clinical practice.[19,43,44]

Herein, we have provided evidence for an alternative non-cellular approach for the treatment of AHF, based on the use of secreted exosomes rather than intact MSCs. We designed and applied a comprehensive approach to evaluate the effects of exosomes generated by different progenitor cell cultures (AF-MSCs, HPL or HL cells) in a cell-free therapeutic application. Our data demonstrate that administration of these EXO has a profound effect on histological, biochemical, and inflammatory hallmarks of liver injury in a mouse model of AHF induced by CCl₄ administration (Figures 2B and 2C). Interestingly, administration of exosomes derived by the different progenitor cell cultures (AF-MSCs, HPL or HL cells) resulted in similar levels of ALT and AST transaminases, respectively, whereas the overall results of this study (*in vivo*, *ex vivo*, *in vitro* experiments) support HPL-EXO treatment for future applications of liver injury (Figure 7). These data are in accordance with and extend recent studies supporting the antiinflammatory and antiapoptotic role of MSC-EXO in experimental models of ischemia-reperfusion injury (IRI) in liver, acute hepatitis, and AHF.[45–48]

We performed proteomic profiling of the AF-MSC-EXO, HPL-EXO, and HL-EXO cargoes to identify common mediators of the protective effects of EXO on AHF. This analysis resulted in a set of 6 proteins that are present in all three EXO types, predicted to be involved in ECM organization, non-integrin membrane-ECM interactions, posttranslation protein phosphorylation, and complement/inflammatory cascades. Among these proteins, MFGE-8, also known as lactadherin, was selected for functional analysis. MFGE-8 is a soluble glycoprotein consisting of N-terminal notch-like EGF domains that serves as a bridge between aᵥβ₃ and aᵥβ₅ integrins on phagocytes and apoptotic cells.[32,49] The hepatoprotective role of MFGE-8 has been indicated in a recent study, suggesting that MFGE-8, secreted by MSCs, regulates TGF-β expression and confers antifibrotic effects in mice with CCl₄ and thioacetamide-induced liver fibrosis.[31] Furthermore, MFGE-8 has been reported to suppress lipid accumulation and inflammation in liver steatosis[30] and metabolic disorders[50] and to reduce the IRE1α/ASK1/JNK apoptosis pathway in mouse models of liver injury, promoting hepatocyte proliferation.[51] It has also been suggested that the reduced serum levels of MFGE-8 in patients with HCC or metabolic
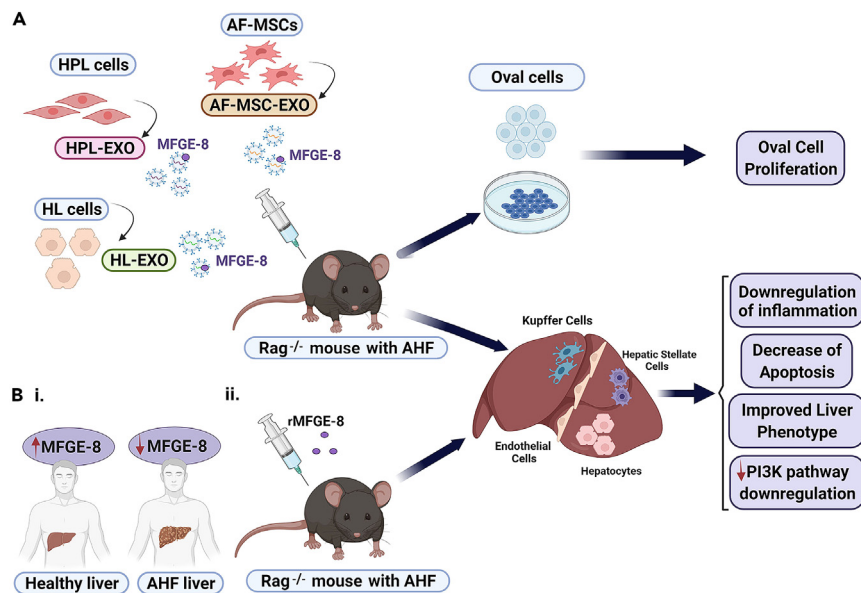
Figure 7. Schematic illustration of AF-MSC-EXO, HPL-EXO, HL-EXO, or rMFGE-8 treatment in CCl4-mice

(A) The AF-MSC-EXO, HPL-EXO, or HL-EXO treatment promoted oval cell proliferation *ex vivo*. The administration of AF-MSC-EXO, HPL-EXO, or HL-EXO in CCl4-induced mice resulted in decrease of apoptosis levels, improvement of the inflammation phenotype, and downregulation of the PI3K pathway.

(B) (i) Higher protein levels of MFGE-8 were detected in liver tissue from healthy donors compared with patients with AHF. (ii) The administration of rMFGE-8 in CCl4-induced mice ameliorated the AHF liver phenotype, decreased apoptosis levels, and downregulated PI3K pathway activity (Created with Biorender.com).

syndrome may serve as a diagnostic and prognostic biomarker.[52,53] Along these lines, hepatic expression of MFGE-8 is reduced in AHF patients, and the CCl4 mouse model of AHF (Figures 5A and 5B) and MFGE-8 expression in liver pericytes correlates with angiogenesis in IRI.[54] Collectively, the aforementioned observations support a generalized protective role of MFGE-8 across several liver pathologies (Figure 7).

Herein, we report increased MFGE-8 levels in both EXO and CM of AF-MSCs and HPL cell cultures that broadly correlate with the therapeutic effects of progenitor cell secretomes on AHF. However, as expected, the administration of EXO is more effective than rMFGE-8 as confirmed by the transaminase levels (AST, ALT), due to the presence of high-quantity proteins, miRNAs, and/or RNAs, also embedded in extracellular vesicles, and their fusion or receptor-based cell membrane interactions, which can also contribute to a more profound therapeutic effect (Figure 7).

Guided by *in silico* prediction of MFGE-8 interacting molecules, we have identified MFGE-8 as a suppressor of the PI3K/AKT pathway. Thus, both MFGE-8-containing EXO and rMFGE-8 downregulate *Akt* and its target *Foxo1*, upregulate the expression of *Pten*, and reduce the levels of the phosphorylated, active form of AKT. Given that inhibition of the PI3K/AKT/mTOR signaling pathway protects against acute hepatic injury induced by Concanavalin-A or LPS/D-galactosamine,[55,56] the aforementioned observations provide a mechanistic framework linking MFGE-8 to hepatoprotection.

In conclusion, the data presented herein expand our knowledge of the biological properties of MSC-EXO and underscore their therapeutic potential in AHF. Our study elucidates the protein cargo of exosomes derived from AF-MSCs and their hepatic progenitors and identifies MFGE-8 as a common effector of their hepatoprotective properties. Our *in silico* and functional analyses suggest that MFGE-8 suppresses the pathogenic PI3K/AKT pathway in the liver and reduces hepatic injury. Collectively, our results suggest an innovative perspective for the management of AHF by using MSC-EXO and MFGE-8, which can also be implemented in other liver diseases (Figure 7).

Limitations of the study

In this study, we identified the cargo of exosomes derived from AF-MSCs and their hepatic progenitors and identified MFGE-8 as a common effector of their hepatoprotective properties.

The major scientific limitation of the current study is the unavailability of patient biopsies with AHF. It is generally impractical to perform invasive liver biopsies to these patients, hence it is difficult to analyze hepatic proteins and transcriptomic changes in long-term recovery. Postmortem collection of liver tissue is usually performed. Secondly, due to the heterogeneity of EV samples, such as EXO, various technical difficulties (such as the cell preconditioning, the cell origin dependency, the lack of high-quality purification protocol of EVs, and their biodistribution) need to be addressed prior to therapeutic applications.

STAR★METHODS

Detailed methods are provided in the online version of this paper and include the following:

SUPPLEMENTAL INFORMATION

Supplemental information can be found online at https://doi.org/10.1016/j.isci.2023.108100.

AUTHOR CONTRIBUTIONS

A.P.: experimental design, *in vitro*, *in vivo*, and *ex vivo* experiments, data analysis and interpretation, manuscript writing, and final approval of manuscript; D.Z.: experimental design, *in vivo* and *ex vivo* experiments, data analysis and interpretation, and final approval of manuscript; L.N.: experimental design, *in vitro* and *ex vivo* experiments, data analysis and interpretation, and final approval of manuscript; M.M.: proteomics data, data analysis and interpretation, manuscript writing, and final approval of manuscript; C.N.: western blot and expression analysis and final approval of manuscript; O.T.: *in vitro* experiments, data analysis, and final approval of manuscript; K.G.: protein analysis and final approval of manuscript; C.K.: proteomics data analysis and final approval of manuscript; I.A.: proteomics data analysis and final approval

of manuscript; A.G.K.: Nanosight analysis; R.G.: human sample provision, manuscript revision, and final approval of manuscript; S.S.: evaluation of human sample IHC and IF analyses and final approval of manuscript; M.X.: exosome isolation and characterization and final approval of the manuscript; A.G.E.: data analysis and interpretation, manuscript revision, and final approval of manuscript; A.V.: proteomics data, data analysis and interpretation, manuscript writing, and final approval of manuscript; M.G.R.: conception and design, financial support, experimental design, data analysis and interpretation, manuscript writing, and final approval of manuscript.

DECLARATION OF INTERESTS

None declared.

REFERENCES

1. Bernal, W., Lee, W.M., Wendon, J., Larsen, F.S., and Williams, R. (2015). Acute liver failure: A curable disease by 2024? J. Hepatol. 62, S112–S120. https://doi.org/10.1016/J.JHEP.2014.12.016.

2. Fiegel, H.C., Kaufmann, P.M., Bruns, H., Kluth, D., Horch, R.E., Vacanti, J.P., and Kneser, U. (2008). Hepatic tissue engineering: from transplantation to customized cell-based liver directed therapies from the laboratory. J. Cell Mol. Med. 12, 56–66. https://doi.org/10.1111/J.1582-4934.2007.00162.X.

3. Stravitz, R.T., and Kramer, D.J. (2009). Management of acute liver failure. Nat. Rev. Gastroenterol. Hepatol. 6, 542–553. https://doi.org/10.1038/nrgastro.2009.127.

4. Slack, A., Hogan, B.J., and Wendon, J. (2018). Acute Hepatic Failure. Liver Anesthesiol. Crit. Care Med. 4, 41–66. https://doi.org/10.1007/978-3-319-64298-7.

5. Mendizabal, M., and Silva, M.O. (2016). Liver transplantation in acute liver failure: A challenging scenario. World J. Gastroenterol. 22, 1523–1531. https://doi.org/10.3748/WJG.V22.I4.1523.

6. Jha, A.K. (2022). Hepatitis of unknown origin in children : Updated evidence and concise review. J. Viral Hepat. 29, 942–947. https://doi.org/10.1111/jvh.13743.

7. Kumar, R., Anand, U., and Priyadarshi, R.N. (2021). Liver transplantation in acute liver failure: Dilemmas and challenges. World J. Transplant. 11, 187–202. https://doi.org/10.5500/WJT.V11.I6.187.

8. Zhou, R., Li, Z., He, C., Li, R., Xia, H., Li, C., Xiao, J., and Chen, Z.Y. (2014). Human umbilical cord mesenchymal stem cells and derived hepatocyte-like cells exhibit similar therapeutic effects on an acute liver failure mouse model. PLoS One 9, e104392. https://doi.org/10.1371/journal.pone.0104392.

9. Wang, Y.H., Wu, D.B., Chen, B., Chen, E.Q., and Tang, H. (2018). Progress in mesenchymal stem cell-based therapy for acute liver failure. Stem Cell Res. Ther. 9, 227. https://doi.org/10.1186/s13287-018-0972-4.

10. Zhou, T., Yuan, Z., Weng, J., Pei, D., Du, X., He, C., and Lai, P. (2021). Challenges and advances in clinical applications of mesenchymal stromal cells. J. Hematol. Oncol. 14, 24. https://doi.org/10.1186/s13045-021-01037-x.

11. Liu, W.h., Song, F.q., Ren, L.n., Guo, W.q., Wang, T., Feng, Y.x., Tang, L.j., and Li, K. (2015). The multiple functional roles of mesenchymal stem cells in participating in treating liver diseases. J. Cell Mol. Med. 19, 511–520. https://doi.org/10.1111/JCMM.12482.

12. Roubelakis, M.G., Pappa, K.I., Bitsika, V., Zagoura, D., Vlahou, A., Papadaki, H.A., Antsaklis, A., and Anagnou, N.P. (2007). Molecular and proteomic characterization of human mesenchymal stem cells derived from amniotic fluid: comparison to bone marrow mesenchymal stem cells. Stem Cell. Dev. 16, 931–952. https://doi.org/10.1089/scd.2007.0036.

13. Trohatou, O., and Roubelakis, M.G. (2017). Mesenchymal stem/stromal cells in regenerative medicine: Past, present, and future. Cell. Reprogr. 19, 217–224. https://doi.org/10.1089/CELL.2016.0062.

14. Zagoura, D., Trohatou, O., Makridakis, M., Kollia, A., Kokla, N., Mokou, M., Psaraki, A., Eliopoulos, A.G., Vlahou, A., and Roubelakis, M.G. (2019). Functional secretome analysis reveals Annexin-A1 as important paracrine factor derived from fetal mesenchymal stem cells in hepatic regeneration. EBioMedicine 45, 542–552. https://doi.org/10.1016/j.ebiom.2019.07.009.

15. Luan, Y., Kong, X., and Feng, Y. (2021). Mesenchymal stem cells therapy for acute liver failure: Recent advances and future perspectives. Liver Res. 5, 53–61. https://doi.org/10.1016/j.livres.2021.03.003.

16. Zagoura, D.S., Roubelakis, M.G., Bitsika, V., Trohatou, O., Pappa, K.I., Kapelouzou, A., Antsaklis, A., and Anagnou, N.P. (2012). Therapeutic potential of a distinct population of human amniotic fluid mesenchymal stem cells and their secreted molecules in mice with acute hepatic failure. Gut 61, 894–906. https://doi.org/10.1136/gutjnl-2011-300908.

17. Phinney, D.G., and Pittenger, M.F. (2017). Concise Review: MSC-derived exosomes for cell-free therapy. Stem Cell. 35, 851–858. https://doi.org/10.1002/stem.2575.

18. Ding, J., Wang, J., and Chen, J. (2021). Exosomes as therapeutic vehicles in liver diseases. Ann. Transl. Med. 9, 735. https://doi.org/10.21037/atm-20-5422.

19. Psaraki, A., Ntari, L., Karakostas, C., Korrou-Karava, D., and Roubelakis, M.G. (2022). Extracellular vesicles derived from Mesenchymal Stem/Stromal cells: the regenerative impact in liver diseases. Hepatology 75, 1590–1603. https://doi.org/10.1002/hep.32129.

20. Liu, W., Yu, M., Xie, D., Wang, L., Ye, C., Zhu, Q., Liu, F., and Yang, L. (2020). Melatonin-stimulated MSC-derived exosomes improve diabetic wound healing through regulating macrophage M1 and M2 polarization by targeting the PTEN/AKT pathway. Stem Cell Res. Ther. 11, 259–315. https://doi.org/10.1186/s13287-020-01756-x.

21. Wen, S., Dooner, M., Cheng, Y., Papa, E., Del Tatto, M., Pereira, M., Deng, Y., Goldberg, L., Aliotta, J., Chatterjee, D., et al. (2016). Mesenchymal stromal cell-derived extracellular vesicles rescue radiation damage to murine marrow hematopoietic cells. Leukemia 30, 2221–2231. https://doi.org/10.1038/LEU.2016.107.

22. Bernardi, S., and Balbi, C. (2020). Extracellular vesicles: From biomarkers to therapeutic tools. Biology 9, 258–266. https://doi.org/10.3390/biology9090258.

23. Bunggulawa, E.J., Wang, W., Yin, T., Wang, N., Durkan, C., Wang, Y., and Wang, G. (2018). Recent advancements in the use of exosomes as drug delivery systems. J. Nanobiotechnol. 16, 81. https://doi.org/10.1186/s12951-018-0403-9.

24. Trohatou, O., Zagoura, D., Orfanos, N.K., Pappa, K.I., Marinos, E., Anagnou, N.P., and Roubelakis, M.G. (2017). miR-26a mediates adipogenesis of amniotic fluid mesenchymal stem/stromal cells via PTEN, Cyclin E1, and CDK6. Stem Cell. Dev. 26, 482–494. https://doi.org/10.1089/scd.2016.0203.

25. Roubelakis, M.G., Bitsika, V., Zagoura, D., Trohatou, O., Pappa, K.I., Makridakis, M., Antsaklis, A., Vlahou, A., and Anagnou, N.P. (2011). In vitro and in vivo properties of distinct populations of amniotic fluid mesenchymal progenitor cells. J. Cell Mol. Med. 15, 1896–1913. https://doi.org/10.1111/j.1582-4934.2010.01180.x.

26. Zagoura, D.S., Trohatou, O., Bitsika, V., Makridakis, M., Pappa, K.I., Vlahou, A., Roubelakis, M.G., and Anagnou, N.P. (2013). AF-MSCs fate can be regulated by culture conditions. Cell Death Dis. 4, e571. https://doi.org/10.1038/cddis.2013.93.

27. Katifelis, H., Filidou, E., Psaraki, A., Yakoub, F., Roubelakis, M.G., Tarapatzi, G., Vradelis, S., Bamias, G., Kolios, G., and Gazouli, M. (2022). Amniotic fluid-derived mesenchymal stem/stromal cell-derived secretome and exosomes improve inflammation in human intestinal subepithelial myofibroblasts. Biomedicines 10, 2357. https://doi.org/10.3390/biomedicines10102357.

28. Yin, C., and Heit, B. (2021). Cellular responses to the efferocytosis of apoptotic cells. Front.

Immunol. *12*, 1–12. https://doi.org/10.1172/JCI77014, 2021.631714.

29. Wang, X., Bu, H.F., Zhong, W., Asai, A., Zhou, Z., and Tan, X.D. (2013). MFG-E8 and HMGB1 are involved in the mechanism underlying alcohol-induced impairment of macrophage efferocytosis. Mol. Med. *19*, 170–182. https://doi.org/10.2119/molmed.2012.00260.

30. Zhang, L., Tian, R., Yao, X., Zhang, X.J., Zhang, P., Huang, Y., She, Z.G., Li, H., Ji, Y.X., and Cai, J. (2021). Milk fat globule–epidermal growth factor–Factor 8 improves hepatic steatosis and inflammation. Hepatology *73*, 586–605. https://doi.org/10.1002/hep.31277.

31. An, S.Y., Jang, Y.J., Lim, H.J., Han, J., Lee, J., Lee, G., Park, J.Y., Park, S.Y., Kim, J.H., Do, B.R., et al. (2017). Milk fat globule-EGF Factor 8, secreted by mesenchymal stem cells, protects aqgainst liver fibrosis in mice. Gastroenterology *152*, 1174–1186. https://doi.org/10.1053/j.gastro.2016.12.003.

32. Thanati, F., Karatzas, E., Baltoumas, F.A., Stravopodis, D.J., Eliopoulos, A.G., and Pavlopoulos, G.A. (2021). Flame: A web tool for functional and literature enrichment analysis of multiple gene lists. Biology *10*, 665–712. https://doi.org/10.3390/biology10070665.

33. Foo, J.B., Looi, Q.H., Chong, P.P., Hassan, N.H., Yeo, G.E.C., Ng, C.Y., Koh, B., How, C.W., Lee, S.H., and Law, J.X. (2021). Comparing the therapeutic Potential of stem cells and their secretory products in regenerative medicine. Stem Cell. Int. *2021*, 2616807. https://doi.org/10.1155/2021/2616807.

34. Nikokiraki, C., Psaraki, A., and Roubelakis, M.G. (2022). The potential clinical use of stem/progenitor cells and organoids in liver diseases. Cells *21*, 1410. https://doi.org/10.3390/cells11091410.

35. Ahangar, P., Mills, S.J., and Cowin, A.J. (2020). Mesenchymal stem cell secretome as an emerging cell-free alternative for improving wound repair. Int. J. Mol. Sci. *21*, 7038–7115. https://doi.org/10.3390/ijms21197038.

36. Damania, A., Jaiman, D., Teotia, A.K., and Kumar, A. (2018). Mesenchymal stromal cell-derived exosome-rich fractionated secretome confers a hepatoprotective effect in liver injury. Stem Cell Res. Ther. *9*, 31. https://doi.org/10.1186/s13287-017-0752-6.

37. Rao, D., Huang, D., Sang, C., Zhong, T., Zhang, Z., and Tang, Z. (2021). Advances in mesenchymal stem cell-derived exosomes as drug delivery vehicles. Front. Bioeng. Biotechnol. *9*, 797359. https://doi.org/10.3389/fbioe.2021.797359.

38. Carlomagno, C., Giannasi, C., Niada, S., Bedoni, M., Gualerzi, A., and Brini, A.T. (2021). Fingerprint of extracellular vesicles and conditioned media for the reproducibility assessment of cell-free therapeutics. Front. Bioeng. Biotechnol. *9*, 640617. https://doi.org/10.3389/fbioe.2021.640617.

39. Bhome, R., Del Vecchio, F., Lee, G.H., Bullock, M.D., Primrose, J.N., Sayan, A.E., and Mirnezami, A.H. (2018). Exosomal microRNAs (ExomiRs): Small molecules with a big role in cancer. Cancer Lett. *420*, 228–235. https://doi.org/10.1016/j.canlet.2018.02.002.

40. Cheng, L., Sharples, R.A., Scicluna, B.J., and Hill, A.F. (2014). Exosomes provide a protective and enriched source of miRNA for biomarker profiling compared to intracellular

and cell-Free blood. J. Extracell. Vesicles *3*, 1–14. https://doi.org/10.3402/jev.v3.23743.

41. Li, X., Corbett, A.L., Taatizadeh, E., Tasnim, N., Little, J.P., Garnis, C., Daugaard, M., Guns, E., Hoorfar, M., and Li, I.T.S. (2019). Challenges and opportunities in exosome research-perspectives from biology, engineering, and cancer therapy. APL Bioeng. *3*, 011503. https://doi.org/10.1063/1.5087122.

42. Dang, X.T.T., Kavishka, J.M., Zhang, D.X., Pirisinu, M., and Le, M.T.N. (2020). Extracellular vesicles as an efficient and versatile system for drug delivery. Cells *9*, 2191. https://doi.org/10.3390/cells9102191.

43. Lou, G., Chen, Z., Zheng, M., and Liu, Y. (2017). Mesenchymal stem cell-derived exosomes as a new therapeutic strategy for liver diseases. Exp. Mol. Med. *49*, e346. https://doi.org/10.1038/emm.2017.63.

44. Villata, S., Canta, M., and Cauda, V. (2020). Evs and bioengineering: From cellular products to engineered nanomachines. Int. J. Mol. Sci. *21*, 6048–6132. https://doi.org/10.3390/ijms21176048.

45. Yadav, P., Trehanpati, N., Maiwall, R., Sehgal, R., Singh, R., Islam, M., Jagdish, R.K., Vijayaraghavan, R., Maheshwari, D., Bhat, S., et al. (2022). Soluble factors and suppressive monocytes can predict early development of sepsis in acute-chronic liver failure. Hepatol. Commun. *6*, 2105–2120. https://doi.org/10.1002/hep4.1949.

46. Anger, F., Camara, M., Ellinger, E., Germer, C.T., Schlegel, N., Otto, C., and Klein, I. (2019). Human mesenchymal stromal cell-derived extracellular vesicles improve liver regeneration after ischemia reperfusion injury in mice. Stem Cell. Dev. *28*, 1451–1462. https://doi.org/10.1089/scd.2019.0085.

47. Sun, C.K., Chen, C.H., Chang, C.L., Chiang, H.J., Sung, P.H., Chen, K.H., Chen, Y.L., Chen, S.Y., Kao, G.S., Chang, H.W., et al. (2017). Melatonin treatment enhances therapeutic effects of exosomes against acute liver ischemia-reperfusion injury. Am. J. Transl. Res. *9*, 1543–1560.

48. Tamura, R., Uemoto, S., and Tabata, Y. (2016). Immunosuppressive effect of mesenchymal stem cell-derived exosomes on a concanavalin A-induced liver injury model. Inflamm. Regen. *36*, 26. https://doi.org/10.1186/s41232-016-0030-5.

49. Verma, A.K., Ali, S.A., Singh, P., Kumar, S., and Mohanty, A.K. (2021). Transcriptional repression of MFG-E8 causes disturbance in the homeostasis of cell cycle through DOCK/ZP4/STAT signaling in buffalo mammary epithelial cells. Front. Cell Dev. Biol. *9*, 568660. https://doi.org/10.3389/fcell.2021.568660.

50. Khalifeh-Soltani, A., McKleroy, W., Sakuma, S., Kevin Tharp, Y.Y.C., Qiu, Y., Turner, S.M., Chawla, A., Stahl, A., and Atabai, K. (2014). Mfge8 promotes obesity by mediating the uptake of dietary fats and serum fatty acids. Nat. Med. *44*, 161–170. https://doi.org/10.1016/j.achaem.2013.07.023.Quo.

51. Li, H., Zhang, T., Wang, K., Lu, M., Guo, Y., Zhang, Y., Chen, Z.N., and Bian, H. (2019). MFGE8 protects against CCl4-induced liver injury by reducing apoptosis and promoting proliferation of hepatocytes. J. Cell. Physiol. *234*, 16463–16474. https://doi.org/10.1002/jcp.28314.

52. Shimagaki, T., Yoshio, S., Kawai, H., Sakamoto, Y., Doi, H., Matsuda, M., Mori, T., Osawa, Y., Fukai, M., Yoshida, T., et al. (2019).

Serum milk fat globule-EGF factor 8 (MFG-E8) as a diagnostic and prognostic biomarker in patients with hepatocellular carcinoma. Sci. Rep. *9*, 15788–15812. https://doi.org/10.1038/s41598-019-52356-6.

53. Lee, H.A., Lim, J., Joo, H.J., Lee, Y.S., Jung, Y.K., Kim, J.H., An, H., Yim, H.J., Jeen, Y.T., Yeon, J.E., et al. (2021). Serum milk fat globule-egf factor 8 protein as a potential biomarker for metabolic syndrome. Clin. Mol. Hepatol. *27*, 463–473. https://doi.org/10.1016/j.biopha.2017.05.037. 10.3350/cmh.2020.0351.

54. Uchiyama, A., Yamada, K., Perera, B., Ogino, S., Yokoyama, Y., Takeuchi, Y., Ishikawa, O., and Motegi, S.I. (2015). Protective Effect of MFG-E8 after cutaneous ischemia-reperfusion injury. J. Invest. Dermatol. *135*, 1157–1165. https://doi.org/10.1038/jid.2014.515.

55. Li, Y., Lu, L., Luo, N., Wang, Y.Q., and Gao, H.M. (2017). Inhibition of PI3K/AKt/mTOR signaling pathway protects against D-galactosamine/lipopolysaccharide-induced acute liver failure by chaperone-mediated autophagy in rats. Biomed. Pharmacother. *92*, 544–553. https://doi.org/10.1016/j.biopha.2017.05.037.

56. Wang, S., Huang, Z., Lei, Y., Han, X., Tian, D., Gong, J., and Liu, M. (2022). Celastrol alleviates autoimmune hepatitis through the PI3K/AKT signaling pathway based on network pharmacology and experiments. Front. Pharmacol. *13*, 816350. https://doi.org/10.3389/fphar.2022.816350.

57. Maugham, M.L., Thomas, P.B., Crisp, G.J., Philp, L.K., Shah, E.T., Herington, A.C., Chen, C., Gregory, L.S., Nelson, C.C., Seim, I., et al. (2017). Insights from engraftable immunodeficient mouse models of hyperinsulinaemia. Sci. Rep. *7*, 491.

58. Barnhoorn, M.C., Plug, L., Jonge, E.S.M.M., Molenkamp, D., Bos, E., Schoonderwoerd, M.J.A., Corver, W.E., van der Meulen-de Jong, A.E., Verspaget, H.W., and Hawinkels, L.J.A.C. (2020). Mesenchymal stromal cell–derived exosomes contribute to epithelial regeneration in experimental inflammatory bowel disease. Cell. Mol. Gastroenterol. Hepatol. *9*, 715–717.e8. https://doi.org/10.1016/j.jcmgh.2020.01.007.

59. Varderidou-Minasian, S., and Lorenowicz, M.J. (2020). Mesenchymal stromal/stem cell derived extracellular vesicles in tissue repair: Challenges and opportunities. Theranostics *10*, 5979–5997. https://doi.org/10.7150/thno.40122.

60. Mantsiou, A., Makridakis, M., Fasoulakis, K., Katafigiotis, I., Constantinides, C.A., Zoidakis, J., Roubelakis, M.G., Vlahou, A., and Lygirou, V. (2020). Proteomics analysis of formalin fixed paraffin embedded tissues in the investigation of prostate cancer. J. Proteome Res. *19*, 2631–2642. https://doi.org/10.1021/acs.jproteome.9b00587.

61. Makridakis, M., and Vlahou, A. (2018). GeLC-MS: A sample Ppeparation method for proteomics analysis of minimal amount of tissue. Methods Mol. Biol. *1788*, 165–175. https://doi.org/10.1007/7651_2017_76.

62. Bindea, G., Mlecnik, B., Hackl, H., Charoentong, P., Tosolini, M., Kirilovsky, A., Fridman, W.H., Pagès, F., Trajanoski, Z., and Galon, J. (2009). ClueGO: a Cytoscape plug-in to decipher functionally grouped gene ontology and pathway annotation networks. Bioinformatics *25*, 1091–1093. https://doi.org/10.1093/bioinformatics/btp101.

STAR★METHODS

KEY RESOURCES TABLE

REAGENT or RESOURCE	SOURCE	IDENTIFIER
Antibodies		
Flotilin1	Santa Cruz Biotechnology, Texas, USA	Cat#sc-74566; RRID:AB_2106563
CD63	Santa Cruz Biotechnology, Texas, USA	Cat#sc-74556; RRID:AB_627877
CD9	Santa Cruz Biotechnology, Texas, USA	Cat#sc-13118; RRID:AB_627213
GRP94	Santa Cruz Biotechnology, Texas, USA	Cat#sc-32249; RRID:AB_627676
MFGE-8	Santa Cruz Biotechnology, Texas, USA	Cat#sc-271574; RRID:AB_10650094
AKT	Upstate, NY, USA	Cat#07-416; RRID:AB_310598
p-AKT	Cell Signaling Technology Inc, Danvers, USA	Cat#9271; RRID:AB_2315049
PTEN	Cell Signaling Technology Inc, Danvers, USA	Cat#9552; RRID:AB_10694066
pPTEN	Cell Signaling Technology Inc, Danvers, USA	Cat#9554; RRID:AB_331411
GAPDH	Santa Cruz Biotechnology, Texas, USA	Cat#sc-32233; RRID:AB_627679
CD24-FITC	Becton Dickinson Biosciences, USA	Cat#555427
Anti-mouse HRP conjugated	Sigma Aldrich LTd, Missouri, USA	Cat#12-349; RRID:AB_390192
Anti-Rabbit HRP conjugated	Sigma Aldrich LTd, Missouri, USA	Cat#12-348; RRID:AB_390191
AlexaFluor 488	Invitrogen, Massachusetts, USA	Cat#A-11029; RRID:AB_2534088
Negative Control IgG1	DAKO (Agilent), Glostrup, Denmark	Cat#XO931; RRID:AB_2889134
Biological samples		
Human acute liver biopsies (blocks)	First Laboratory of Pathology, Medical School, NKUA, Greece and Clinical Pathology and Pathology Division, Karolinska Institute, Sweden	HHSN267200700004CN01-DK-7-0004
Primary Amniotic fluid MSCs (AF-MSCs)	Patients derived from Alexandra Hospital, Athens, Greece	N/A
Chemicals, peptides, and recombinant proteins		
rMFGE-8	R&D Systems, Minneapolis, MN,USA	2767-MF-050
CellTiter 96 Aqueous One Solution Assay	Promega, Madison, Winsconsin, USA	G3582
Sheep-anti-RatIgG Dynabeads	Invitrogen, Massachusetts,USA	11035
DMEM	Gibco, Massachusetts, USA	41966-029
FBS	PAN-BIOTECH	P30-19375

(Continued on next page)

Continued

REAGENT or RESOURCE	SOURCE	IDENTIFIER
PBS	Gibco, Massachusetts,USA	Cat#14190144
Iscove's modified Dulbeco medium-IMDM	Gibco, Massachusetts,USA	Cat#31980022
EGF	Peprotech, London, UK	AF-100-15
bFGF	Peprotech, London, UK	100-18B-10μG
HGF	Peprotech, London, UK	100-39-10μG
Oncostatin M	Peprotech, London UK	300-10-10μG
Dexamethasone	Sigma-Aldrich Ltd. Ltd. Missouri, USA	D2915
ITS Liquid Media Supplement (100×)	Sigma-Aldrich Ltd., Missouri, USA	I3146
DAPI	Biotium, France	Cat#40043
Dako fluorescent Mounting Medium	Dako North America, Inc., CA, USA	Cat#53028
Xylene	Carlo-Erba Reagents, Cornaredo, Italy	LA113580F
Harris Hematoxylene	H&E, VWR, Lutterworth, UK	MFCD00078111
1% eosin (H&E, VWR,	Lutterworth, UK	MFCD00005040
4% formalin	Sigma-Aldrich Ltd., Missouri, USA	1.00496
Nucleospin total RNA FFPE XS	MN, Germany	Cat#740969
PVDF membranes	MN, Germany	Cat#741260
TUNEL apoptosis Assay Kit (HRP-DAB)	AssayGenie, Dublin 2	ES00331-20
Oil Red O powder	Sigma Aldrich, Missouri, USA	00625-25G
ECL (Luminata Forte)	Millipore, Massachusetts, USA	WBLUF0100
DMSO	Sigma Aldrich Ltd., Missouri, USA	
Critical commercial assays		
Envision flex+ mouse high PH kit	Dako, Glostrup, Denmark,Qiagen, Hilden, Germany	K3468
Periodic Acid-Schiff (PAS) stain	Sigma-Aldrich Ltd, Missouri, USA	395B
PKH26-RED FLUORESCENT CELL LINKER	Merck-Millipore, USA	MINI26-1KT
Deposited data		
Dataset Identifier: MSV000092848	MassIVE (Mass Spectrometry Interactive Virtual Environment)	https://massive.ucsd.edu/ProteoSAFe/static/massive.jsp)
Experimental models: Organisms/strains		
Rag $^{-/-}$ mouse	Animal Facility of the BRFAA, Athens, Greece (Maugham et al. Scientific Reports, 2016)	https://www.jax.org/
Oligonucleotides		
PI3K/p85 FW 5'-GCAGAGGGCTACCAGTACAGA-3' RV 5'-CTGAATCCAAGTGCCACTAAGG-3'	Primer Bank https://pga.mgh.harvard.edu/primerbank/	1621040a1
MTOR FW 5'-ACCGGCACACATTTGAAGAAG-3' RV 5'-CTCGTTGAGGATCAGCAAGG-3'	Primer Bank https://pga.mgh.harvard.edu/primerbank/	9910228a1
PTEN FW5'-TTTGCTAGTGAGTGGAATCCTCT-3' RV 5-TGTGACAAAAGTGACACAGATCA-3'	Primer Bank https://pga.mgh.harvard.edu/primerbank/	28893025a1
IL-1b FW 5'-CAGGTCGCTCAGGGTCACA-3' RV 5'-CAGAGGCAAGGAGGAAACACA-3'	Primer Bank https://pga.mgh.harvard.edu/primerbank/	N/A

Continued

REAGENT or RESOURCE	SOURCE	IDENTIFIER
BCL-2 FW 5′-GTCGCTACCGTCGTGACTTC-3′ RV 5′- CAGACATGCACCTACCCAGC-3′	Primer Bank https://pga.mgh.harvard.edu/primerbank/	28916685a1
PPARG FW- 5′TTTTCCGAAGAACCATCCGATT-3′ RV 5′-ATGGCATTGTGAGACATCCCC-3′	Primer Bank https://pga.mgh.harvard.edu/primerbank/	187960104c3
MFGE8 FW 5′-AGATGCGGGTATCAGGTGTGA-3′ RV 5′-GGGGCTCAGAACATCCGTG-3′	Primer Bank https://pga.mgh.harvard.edu/primerbank/	28070929a1
FOXO1 FW 5′-ATGCTCAATCCAGAGGGAGG-3′ RV 5′-ACTCGCAGGCCACTTAGAAAA-3′	Primer Bank https://pga.mgh.harvard.edu/primerbank/	239985491c2
TNF-a FW 5′-GACGTGGAACTGGCAGAAGAG RV 5′-TTGGTGGTTTGTGAGTGTGAG	Primer Bank https://pga.mgh.harvard.edu/primerbank/	202093a1
NLRP3 FW 5′-ATTACCCGCCCGAGAAAGG-3′ RV 5′-TCGCAGCAAAGATCCACACAG-3′	Primer Bank https://pga.mgh.harvard.edu/primerbank/	22003870a1
Software and algorithms		
ClueGO/Cytoscape	Cytoscape App Store *Bindea* et al.[9]	3.5.1 version http://apps.cytoscape.org/apps/cluego
STRING	STRING version 12.0	https://string-db.org/
REACTOME	Reactome Pathway Database	https://reactome.org/
Imaris	Oxford Instruments IMARIS	9.9 version
R software package	The R project for Statistical Computing	https://www.r-project.org/
SPSS software	IBM SPSS software	IBM SPSS Statistics, NY:IBM Corp.,2013
ImageJ-win64	National Institute of Health	N/A
WebGestalt software	*Liao* et al.[8]	2019 version http://www.webgestalt.org
FLAME software	*Thanati* et al.[32]	https://bib.fleming.gr:8084/app/flame
Heatmapper software	Heatmapper *Babicki* et al.[7]	http://www.heatmapper.ca/
G*Power	Universität Düsseldorf: Psychologie - HHU	3.1.9 version
Other		
Biorender.com	Biorender	Scientific Image and Illustration Software | BioRender
Gene Ontology (GO)	The Gene Ontology Resource	http://geneontology.org
Swiss-Prot bank	UniProt	https://www.uniprot.org
REACTOME	Reactome Pathway Database	https://reactome.org/
Morpheus software	N/A	https://clue.io/morpheus

RESOURCE AVAILABILITY

Lead contact

Further information and requests for resources and reagents should be directed to, and will be fulfilled upon reasonable request, by the lead contact, Maria G. Roubelakis. (mailto:roubel@med.uoa.gr).

Materials availability

This study did not generate new unique reagents.

Data and code availability

The authors declare that all relevant data are available within the article and its supplemental information files or from the corresponding author upon reasonable request. The raw data are available on MassIVE (Mass Spectrometry Interactive Virtual Environment) open access repository (https://massive.ucsd.edu/ProteoSAFe/static/massive.jsp) with the Dataset Identifier: MSV000092848. This study did not generate new code.

EXPERIMENTAL MODEL AND STUDY PARTICIPANT DETAILS

Isolation and culture of AF-MSCs

Cultured AF-MSCs were isolated from 6 human AF samples, collected during scheduled normal pregnancy amniocenteses for prenatal diagnosis between the 15th and 18th week of gestation, as described previously.[14,16,24,25] All samples were collected with a written informed consent, following the approval by Ethical Committee of Alexandra Hospital, Athens, Greece, the bioethics committee of the School of Medicine of the NKUA and the BRFAA. Ten-15 ml of amniotic fluid was aspirated for each sample, using a 22G needle and under ultrasonographic control. The procedure-related spontaneous abortion rate ranges from 0.06 to 0.5%. Each sample was centrifuged at 1,300 rpm for 10 min and the pellet was resuspended in Dulbecco's modified Eagle's medium (DMEM; Sigma-Aldrich Ltd., Gillingham, Dorset, UK) supplemented with 20% (vol/vol) fetal bovine serum (FBS) (Gibco-BRL, Paisley, Scotland, UK) in a 25 cm^2 tissue culture-treated flask and incubated at 37°C in a 5% (vol/vol) humidified CO_2 chamber for approximately 10-12 days, when the first colonies appeared. Spindle-shaped colonies from 6 AF-MSCs samples were selected for subculture in the present study.[14,16] Cells were regularly tested for mycoplasma contamination.

Hepatogenic differentiation of AF-MSCs

Spindle shaped AF-MSCs were seeded at 1.5x10^6 / 75xcm^2 flasks and cultured in serum-deprived media (Iscove's modified Dulbeco medium-IMDM, Thermo Fisher Scientific Inc. Gibco, Massachusetts, USA) for 2 days supplemented with 20ng/ml epidermal growth factor (EGF, Peprotech, London, UK) and 10ng/ml basic fibroblast growth factor (bFGF, Peprotech, London, UK). To induce the HPL differentiation, cells were cultured with IMDM supplemented with 20ng/ml hepatocyte growth factor (HGF, Peprotech, London, UK), 10ng/ml bFGF and 0.1% dimethyl sulfoxide (DMSO, Sigma Aldrich Ltd., Missouri, USA) for another 7 days. These cells were defined as Hepatic Progenitor-Like cells (HPL cells). To further differentiate HPL cells into Hepatocyte-Like cells (HL cells), HPL cells were cultured with IMDM supplemented with 20ng/ml oncostatin M (Peprotech, London UK), 1μM dexamethasone (Sigma-Aldrich Ltd. Ltd. St. Louis. MO, USA) and 50μg/ml ITS+ (Sigma-Aldrich Ltd., Missouri, USA) for 2 weeks. The evaluation of hepatogenic differentiation was conducted as previously reported with Periodic Acid-Schiff (PAS) stain (Sigma-Aldrich Ltd, Missouri, USA) and photographs (20x) were taken using an inverted microscope Leica BMIRE2.[16]

EXO isolation and characterization

For EXO isolation, 7.5x10^6 AF-MSCs, HPL- and HL-cells were cultured until 90% confluency for 48h in DMEM supplemented with EXO-depleted FBS at a final concentration 0.5%. Serum EXO depletion was performed by centrifuging at 100,000g for 16h. Twenty-four hours later CM (45ml CM from each cell type) were collected and centrifuged at 1,000g for 5min to remove cell debris and then at 2,000g for 15min to remove apoptotic bodies. The supernatant was then concentrated, using ultrafiltration units (3kDa cutoff) and centrifuged (SORVALL/100SE, MA, USA) at 100,000g for 2h at 4°C. Pellets were re-suspended in PBS (Thermo Fisher Scientific Inc., Massachusetts, USA) and stored at -20°C. The supernatant was used as a negative control (EXO-control). Protein concentration was estimated by Bradford assay (BioRad Laboratories Inc., CA, USA).[27]

Animal model and administration of CM, EXO or rMFGE-8

Female *Rag*$^{-/-}$ mice (6-8 weeks old) were housed and maintained at the Animal Facility of the BRFAA. Rag 1-/- mice are immunodeficient and are prone to serious metabolic disorders under specific circumstances. In particular they exert hyperinsulinemia, insulin resistance, high lipogenesis, hepatic steatosis and intracellular lipid accumulation, which make them a suitable mouse model for the study of liver disorders[57] (Data S2). Liver damage was observed to a greater extend in female compared to male mice during the establishment of the disease model. The facility is registered as "breeding" and "experimental" facility (Reg. Numbers: EL BIO 01 and EL 25 BIO 03, respectively) according to the Greek Presidential Decree 56/2013, which harmonizes National Legislation with the European Directive 2010/63 on the protection of animals used for scientific purposes. The procedures for the care and treatment of animals were performed according to the Institutional guidelines, which follow the guidelines of the Association for Assessment and Accreditation of Laboratory of Animal Care (AAALAC) (Approval No.3373/ 03-07-2018 and No.350028/20-04-22), the recommendations of FELASA and NIH (Data S2).

The study protocol was approved by the Department of Agriculture and Veterinary Service of the Prefecture of Athens (Permit Number: 6653/ 17-12-2015). Cages were kept in the same animal room with HEPA filtered air supply, 15 ACH, light intensity of 300 lux measured one meter above the floor in the middle of the room and color temperature of 4100K as well as positive air pressure of 0.6Pa within the room. Room conditions were continuously monitored through the central Building Management System (BMS) of the animal facility. Animals were bred and maintained in a specific pathogen-free, temperature-and humidity-regulated unit (21 ± 2°C; 55% ± 10%), and a 12/12 h light/dark cycle with lights off at 19:00h and no twilight period. Mice were housed in individually ventilated cages (IVC) (Seal Safe 1284 L, H-Temp™, Techniplast,Varese, Italy) receiving 70 air changes per hour, at a stocking density of 4–5 mice per cage unless otherwise stated [caging dimensions (LxWxH): 365 × 207 × 14mm floor area = 530cm^2]. All mice had *ad libitum* access to filtered tap water in drinking bottles and a vacuum-packed pelleted rodent

chow that contained 18.5% protein, 5.5% fat, 4.5% fiber, and 6% ash (4RF22, Mucedola, Milan, Italy). The bedding in each cage comprised of ~250g of autoclaved corncob bedding (Rehofix MK 2000, J. Rettenmaier & So, Rosenberg, Germany). The cages were cleaned and autoclaved once a week (Data S2).

Additionally, the calculation of the total mouse number required for the experimental procedure was performed by using G*Power 3.1.9 software in conjunction with ANOVA: Fixed effects, omnibus, one-way statistical analysis. Since there was not sufficient data in previous publications for the Effect size, it was determined *a priori*: Compute required sample size, with Input: Effect size f=0.4. The proposed protocol is mild to moderate in severity by design. There are no procedures that cause particular pain and stress. The injections of EXO or CM, as well as of rMFGE-8 are short, gentle (i.h. process), do not cause much pain, and performed once. At the same time, biochemical analyzes of serum transaminase levels will be performed after a gentle euthanasia procedure (Data S2).

Briefly, female $Rag^{-/-}$ mice (n=10) were administered intraperitonially (i.p.) a single dose of 0.5 ml/kg body weight CCl4 dissolved in sun oil, whereas control animals (n = 10) received phosphate buffered saline only.[14,16] The following day, mice underwent intrahepatic (i.h.) injection of CM derived from 1.5×10^6 AF-MSC-, HPL- or HL-cells (n=10/group),[14,16] EXO (20μg in PBS) released by AF-MSCs, HPL-or HL-cells (n=10/group) or recombinant human MFGE-8 (rMFGE-8) protein (6.5μg in PBS; 2767-MF-050, R&D Systems, Minnesota, USA) (n=7/group). PBS, DMEM (0.5% FBS), AF-MSC-, HPL- or HL-EXO-depleted-CM (AF-MSC-, HPL- or HL-EXO-control) were used as negative controls, (n=10/group). There were no exclusions in the experimental units or data points in the final analysis. The i.h. injections were performed under the guidance of ultrasound imaging (Ultrasound Vivid7, Georgia, USA) (Data S2).

AF-MSC-, HPL- and HL-EXO were isolated from CM from approximately 1.2×10^7 cells in order to collect 20μg of exosomes. Each mouse with CCl4-induced AHF was injected with a single dose of 20μg EXO, as previously described in a IBD model for *in vivo* and *in vitro* experiments.[58] The total amount of EXO dose/mouse was quantified by NTA at $2.925 \times 10^8 \pm 1.48 \times 10^7$ particles per body as previously described[59] (Data S2).

Human liver specimens

Formalin fixed and Paraffin embedded (FFPE) human liver tissues were obtained from the First Laboratory of Pathology, Medical School, NKUA, Greece, or Clinical Pathology and Pathology Division, Karolinska Institute, Sweden. All human samples were used according to declaration of Helsinki and under an Institutional Review Board–approved protocol and with support from the Liver Tissue Procurement and Distribution System (HHSN 267200700004CN01-DK-7-0004). A policy of strict anonymity and confidentiality was assured according to Ethics Committee. Biopsies from 2 available post-mortem AHF patients (males), as well as, a case with nearly normal liver histology (male) serving as negative control, were analyzed for the validation of MFGE-8 expression.

Ethics approval

Ethics approvals are stated in the respective sections (STAR Methods).

Patient consent for publication

Not applicable.

METHOD DETAILS

Nanoparticle Tracker analysis (NTA) of EXO samples

Nanoparticle tracking analysis (NTA) was performed by the same operator using the NanoSight NS300 instrument (Malvern Instruments, Amesbury, UK). The NanoSight NS300 is equipped with a 532 nm laser (green), a high sensitivity sCMOS camera and a syringe pump. The AF-MSC-, HPL- and HL-EXO samples were diluted in particle-free PBS (0.22 μm filtered) to obtain a concentration within the recommended measurement range ($1–10 \times 10^8$ particles/mL), corresponding to 1:100 dilution of the initial sample concentration. Each EXO-sample was loaded on 1 ml syringe that was then placed to the pump. Autofocus was adjusted so that indistinct particles were avoided. For each measurement, five 30 seconds videos were captured under the following conditions: cell temperature: 25°C; Syringe speed: 100 μl/s. Experiment videos were analysed using NanoSight NTA 3.4 build 3.4.4 software (Copyright 2020, Malvern) after capture in script control mode. A total of 1500 frames were examined per sample.

Western blot (WB) analysis

WB was conducted to evaluate the presence of AF-MSC-, HPL- and HL-EXO. An average of 15μg EXO proteins were separated by 12% SDS-PAGE gels, transferred to PVDF (PVDF membrane for Protein Blotting, BIO-RAD, CA, USA) and blocked in 5% milk in TBST (1X Tris-Buffered Saline PH 7.6, 0.1% Tween) for 1h at room temperature. The membranes were incubated with mouse anti-Flotilin1 (1:1000, sc-133153, Cell Signaling, Texas, USA), mouse anti-CD63 (1:500, SC-5275, Santa Cruz, Texas, USA), mouse anti-CD9 (1:200, sc-13118, Santa Cruz, Texas, USA) and mouse anti-GAPDH (1:1000, MAB374, Millipore, Massachusetts, USA) antibodies overnight at 4°C (Data S1). Three washes with TBST (1X Tris-Buffered Saline PH 7.6, 1% Tween) were followed and membranes were incubated with anti-mouse HRP-conjugated secondary antibody (1:1000, Millipore, Massachusetts, USA) for 1h. Blots were washed 2 times with TBST and 1 time with TBS alone for 10min and the expression signals were visualized by blot detection system (iBright CL1500 Imaging System, Massachusetts, USA), using ECL (Luminata Forte, Millipore, Massachusetts, USA). A volume of approximately 30μl of AF-MSC, HPL or HL-EXO control was used as negative control.

For the detection of AKT, p-AKT, PTEN, p-PTEN (Data S1) protein expression levels in FFPE mouse liver tissues treated with AF-MSC-, HPL, HL-EXO or CM, an average of 50µg protein was used for WB. Tissues from healthy mice were used as negative controls and tissues from mice with AHF as positive controls.

Total protein isolation protocol was conducted for FFPE liver tissues. Briefly, three paraffin sections were used for a single protein extraction followed by deparaffinization, rehydration, resuspension into FASP buffer (100mM Tris-HCl pH 7.6, SDS 4%, 100mM DTE) and 3 cycles x 5sec of sonication. Samples were then heated at 90°C for 1h and were centrifuged at 13000rpm for 10min at RT. The supernatants were transferred at 1.5ml Eppendorf tubes (Amicon, Amicon Ultra 0.5ml 3K, UFC500396, Merck-Millipore, USA) for concentration at a final volume of 60µl and stored at -80°C for future use, according to an established protocol.[60] Protein expression levels from WB were estimated with ImageJ-win 64.

EXO sample preparation for Transmission Electron Microscopy (TEM) imaging

The EXO samples derived from AF-MSC, HPL and HL cells were fixed 1:1 with 4% paraformaldehyde (Sigma Aldrich Ltd., Missouri, USA) overnight at 4°C. Fixed samples of 5 µL were placed onto 300 mesh copper grids with carbon-coated formvar film (Sigma Aldrich Ltd., Missouri, USA) and incubated for 20 min. Brief washes with PBS were followed and grids were incubated with 1% glutaraldehyde for 5min and subsequently washed with dH2O. Afterwards, the grids were stained with uranyl oxalate (pH 7) (Sigma Aldrich Ltd., Missouri, USA) for 5min and methyl cellulose – uranyl acetate (Sigma Aldrich Ltd., Missouri, USA) for 10min on ice. The excess liquid was removed by blotting with Whatman filter paper and the grids were allowed to dry. Samples were examined with a Philips 420 Transmission Electron Microscope at an acceleration voltage of 60 kV and photographed with a Megaview G2 CCD camera (Olympus SIS, Münster, Germany).

EXO labeling

AF-MSC-EXO were labeled with PKH26 dye according to the manufacturers' instructions (MINI26-1KT, Merck-Millipore, USA) and administered via i.h. or intravenous (i.v.) injection into CCl$_4$-mice. Whole liver tissues were visualized by the Xenogen IVIS Lumina II System (Advanced Molecular Vision, Inc., Lincolnshire, UK).

Biochemical analysis for liver function

Mouse heart blood was collected from mice 24h post AF-MSC, HPL-, HL-EXO (n=10 per group), CM (n=10 per group) or rMFGE-8 (n=3 per group) administration and centrifuged at 11,000xg for 5min. The serum samples were collected separately and the levels of AST, and ALT, were estimated by an automatic biochemical analyzer (Medilyzer-Medicon Hellas).

Histochemical analyses of mice liver sections after CM or EXO administration

Twenty-four hours after AF-MSC-, HPL-, HL-EXO or CM, as well as after rMFGE-8 peptide administration mice were sacrificed and liver tissues were fixed in 4% formalin (Sigma-Aldrich Ltd., Missouri, USA) for 24h. Subsequently, liver lobes were washed with tub water for 10min and placed in 70% ethanol. Liver tissues were embedded in paraffin and a five to seven-micron liver sections were prepared. Further, the liver sections were de-waxed in xylene (Carlo-Erba Reagents, Cornaredo, Italy) and rehydrated in graded ethanol. Harris' hematoxylin and 1% eosin (H&E, VWR, Lutterworth, UK) were used for morphological assessment. H&E sections were washed with water and dehydrated with graded alcohol and xylene. Images were obtained by bright-light microscope (Leica DM LS2 microscope, Leica DFC500 digital color camera).

Oil Red O staining

Frozen sections of 5µm from CCl$_4$-induced mice treated with AF-MSC-, HPL- and HL-EXO or -CM, were formalin fixed for 5min and rinsed in 60% isopropanol. Oil Red O staining was followed with Oil Red O working solution [12ml of the filtered stock solution: 0.09g Oil Red O powder (00625-25G Sigma Aldrich, Missouri, USA) in 30ml, was further diluted in 8ml dH2O] for 20min and slides were rinsed in 60% isopropanol. Slides were washed with dH2O and mounting (Dako fluorescent Mounting Medium 53028, Dako North America, Inc., CA, USA) was performed. Liver sections of mice injected with PBS were used as negative controls. Quantification of stained area was measured with Image J v1.43m software.

TUNEL assay

TUNEL assay was performed according to the manufacturers' instructions of TUNEL apoptosis Assay Kit (HRP-DAB) (ES00331-20, AssayGenie, Dublin 2, Ireland) in FFPE liver sections of CCl$_4$- mice treated AF-MSC-, HPL- and HL-EXO or CM (n=3 per group). Liver sections of mice injected with PBS were used as negative controls (n=3 per group). Positive apoptotic cells were counted with Image J v1.43m software.

Immunofluorescence (IF) staining of mouse and human liver sections

FFPE liver tissue sections of 5-7µm from mice treated with EXO or CM or rMFGE-8 derived from AF-MSC, HPL, HL cells, as well as from human specimens with AHF were stained for mouse anti-MFGE-8 (sc-271574, Santa Cruz, Texas, USA). Slides were incubated at 60°C for 30min and deparaffinized in Xylene (Carlo-Erba Reagents, Cornaredo, Italy). Rehydration of the slides was followed with graded ethanol (100%, 95%, 80%, 50% EtOH) and slides were rinsed in H2O. Subsequently, slides were boiled in citrate acid solution (10Mm, PH 6.0) for 10min, immerged in PBS and blocking solution [10% horse serum (16050130, Thermo Fisher Scientific Inc., Massachusetts, USA), 0.1% Triton 1X in PBS] was

applied for 1h at RT. Washes of PBS were followed and slides were incubated overnight with primary antibodies in 1:50 dilution at buffer solution (5 % horse serum and 0.1% Triton 1x in PBS) at 4°C. The following day, slides were washed with PBS and incubated with secondary antibodies of goat anti-mouse AlexaFluor 488 (A-11029, Invitrogen, Massachusetts, USA) for 1h at RT in the dark. DAPI (40043, Biotium, France) staining was performed for 5min and slides were washed with PBS and then mounted with Dako fluorescent Mounting Medium (53028, Dako North America, Inc., CA, USA). Sections derived from mice treated with PBS and from human liver with average steatosis were used as negative controls. Immunofluorescent signals were visualized by a confocal laser scanning microscope (TCS SP5 Confocal System, Leica, Mannheim, Germany), while the quantification of protein expression levels was performed with Image J v1.43m software. The IF negative control was quantified at 2.3 ± 0.24 Median Fluorescence Intensity (MFI) for MFGE-8 expression.

Immunohistochemical staining of human liver sections

Sections of 5-7μm derived from FFPE liver tissues of patient with AHF and control patient were used for immunohistochemical staining of MFGE-8 expression. Sections were de-deparaffinized by Xylene (Carlo-Erba Reagents, Cornaredo, Italy), hydrated with graded ethanol solutions (100%, 96%, 80%, 70%, 50%) and rinsed in TBS (1X Tris-Buffered Saline PH 7.6). Subsequently, slides were boiled with citrate acid buffer (10Mm, PH 6.0) for 10min and blocking with $3\% H_2O_2$ for 30min was followed. The samples were washed in TBS and incubated overnight at 4°C with primary antibody for MFGE-8 in 1:40 (sc-271574, Santa Cruz, USA). The following day, slides were washed in TBS and incubated with anti-mouse HRP-conjugated antibody (1:1000) for 1h at RT in dark. After washing in TBS, DAB was used according to the manufacturers' instructions of Envision flex+ mouse high PH kit (lot 11241346, K3468, Dako, Glostrup, Denmark-Qiagen, Hilden, Germany). The detection of dark brown signal was monitored under light microscope. Slides were then washed in tap water and counterstaining with Hematoxylene (H&E, VWR, Lutterworth, UK) was performed. Slides were also dehydrated with graded ethanol solutions (50%, 70%, 80%, 96%, 100%) and xylene. Images were obtained with bright-light microscope (Leica DM LS2 microscope, Leica DFC500 digital color camera).

Oval cell isolation

Oval cells (CD24$^+$/Ter119$^-$) were isolated from 6-8-week-old Rag$^{-/-}$ (n=6) resected livers derived from CCl$_4$-induced mice. A liver lobe, was resected under sterile conditions from each mouse and then was dissolved through cell strainer (100μm pore size) with simultaneous washes with sterile PBS (Phosphate-Buffered Saline, Thermo Fisher Scientific Inc. Gibco, Massachusetts, USA). Cells were centrifuged at 1,200xrpm for 5min and incubated with RBC 1X buffer [155mM NH4Cl (Sigma-Aldrich, Missouri, USA), 10mM NaHCO$_3$ (Sigma-Aldrich, Missouri, USA), 0.1mM EDTA (Sigma-Aldrich, Missouri, USA)] for 10min at 4°C. The reaction was terminated by FBS in a ratio of 1/10 RBC buffer. Afterwards, cells suspended in PBS buffer (0.1% BSA και 2mM EDTA) were incubated with 25μl rat anti-mouse CD24-FITC antibody (55326, Becton Dickinson Biosciences, USA,) for 30min in a rotary motion at 4°C and centrifuged at 850xg for 8min. A 30min incubation protocol of cells with Sheep anti-Rat IgG Dynabeads (Invitrogen, Massachusetts, USA) in PBS buffer was then followed and oval cells were finally separated using magnet (Invitrogen, Massachusetts, USA). The oval cell isolation was confirmed by FACs assay for CD24$^+$/Ter119$^-$.[14,16]

Oval cell proliferation assay

The oval cell proliferation was determined by MTS assay (Promega Ltd. WI, USA). Oval cells were seeded into a 96 well plate at density of 1,5 x10^4 cells/well in 5 replicates and cultured with AF-MSC-CM, HPL-CM, HL-CM or AF-MSC-EXO, HPL-EXO, HL-EXO, as well as with 0.5 % FBS as negative control for CM, DMEM 20% FBS as positive control and AF-MSC, HPL, HL-EXO controls as negative controls for exosomes, for 1 and 3 days at 37°C. The absorbance for each time point after 2,5 h of incubation with the MTS reagent, was measured at 492nm by an ELISA Reader (Multiskan GO version1.01.10, Thermo Scientific, Massachusetts, USA). The reference wavelength was adjusted at 595nm with an average absorbance at 0.048/well. The proliferation rate was calculated using the formula: [(ODdayx - ODday0)/ODday0 x 100] and the experiment was performed in three replicates. The mean of each experiment was calculated and the results were analyzed with ANOVA test.[14,16]

RNA extraction and RT-PCR

Total RNA was isolated from 7μm liver sections of FFPE liver tissues of CCl$_4$-mice treated with AF-MSC-, HPL-, HL-EXO or -CM as well as with rMFGE-8, according to the manufacturer's instructions (740969, Nucleospin total RNA FFPE XS, MN, Germany). More specifically, 7-8 paraffin sections of 7μm were used for a single RNA extraction. cDNA synthesis was performed using FIREScript RT cDNA Synthesis KIT (06-15-0000S, Solis BioDyne, Estonia) and RT-PCR analysis with 5x HOT FIREPol EvaGreen qPCR Supermix (08-36-0000S, Solis BioDyne, Tartu, Estonia) was conducted for Pi3K-p85, PTEN, FOXO1, mTOR, MFGE-8, Bcl-2, PPARG genes (key resources table), using the detection system SaCycler-96 Real Time PCR System (Sacace Biotechnologies Srl., Como, Italy).

Protein sample preparation for LC MS/MS analysis

Protease inhibitors (Roche) were added at a final concentration of 3.6% and samples were stored at -80°C until further use. Samples were prepared with the In-gel digestion coupled with mass spectrometric (GeLC-MS) method as previously described.[61] In particular, 10 microgram of each sample was analyzed in SDS-PAGE (5% stacking, 12% separating). The electrophoresis was stopped when samples just entered the separating gel and gels were fixed with 30% methanol, 10% acetic acid for 30 min followed by 3 washes with water (3x10min) and stained with Coomassie colloidal blue overnight. Excess of stain was washed with water (3x10min washes). Each band was excised from the gel and further sliced to small pieces (1-2mm). Gel pieces were destained with 40% Acetonitrile, 50mM NH$_4$HCO$_3$ and then reduced with 10mM DTE

in 100mM NH$_4$HCO$_3$ for 20min RT. After reduction, samples were alkylated with 54mM Iodoacetamide in 100mM NH$_4$HCO$_3$ for 20min RT in the dark. Samples were then washed with 100mM NH$_4$HCO$_3$ for 20 min at RT, followed by another wash with 40% Acetonitrile, 50mM NH$_4$HCO$_3$ for 20min at RT and a final wash with ultrapure water under the same conditions was performed. Gel pieces were dried in a centrifugal vacuum concentrator (speed vacuum) and trypsinized overnight in the dark at RT, by adding 600ng of trypsin per sample (trypsin stock solution: 10ng/μL in 10mM NH$_4$HCO$_3$, pH 8.5). Peptides were extracted after incubation with the following buffers: 50mM NH$_4$HCO$_3$ for 15min at RT followed by two incubations with 10% Formic Acid, Acetonitrile (1:1) for 15 min at RT and subsequently were eluted in a final volume of 600μL and filtered with 0.22μm PVDF filers (Merck Millipore, Massachusetts, USA) before dried in a centrifugal vacuum concentrator (speed vac). Dried peptides were reconstituted in mobile phase A buffer (0.1% formic acid, pH 3) and processed with LC-MS/MS analysis (Dionex Ultimate 3000 UHPLC, coupled to a Q Exactive Hybrid Quadrupole-Orbitrap Mass Spectrometer, Thermo Scientific, Massachusetts, USA).

LC-MS/MS analysis

All LC-MS/MS experiments were performed on the Dionex Ultimate 3000 UHPLC system coupled with the high-resolution nano-ESI Q-Exactive mass spectrometer (Thermo Scientific, Massachusetts, USA). Each sample was reconstituted in 10 μL loading solution composed of 0.1 % v/v formic acid. A 5μL volume was injected and loaded on the Acclaim PepMap 100, 100μm × 2cm C 18, 5μm, 100 Å trapping column with the ulPickUp Injection mode with the loading pump operating at flow rate 5 μL/min. For the peptide separation the Acclaim PepMap RSLC, 75 μm × 50 cm, nanoViper, C18, 2 μm, 100 Å columns retrofitted to a PicoTip emitter was used for multi-step gradient elution. Mobile phase (A) was composed of 0.1 % formic acid and mobile phase (B) was composed of 100% acetonitrile, 0.1% formic acid. The peptides were eluted under a 120-minute gradient from 2% (B) to 80% (B). Flow rate was 300 nL/min and column temperature was set at 35°C. Gaseous phase transition of the separated peptides was achieved with positive ion electrospray ionization applying a voltage of 2.5 kV. For every MS survey scan, the top 10 most abundant multiply charged precursor ions between m/z ratio 300 and 2200 and intensity threshold 500 counts were selected with FT mass resolution of 60,000 and subjected to HCD fragmentation. Tandem mass spectra were acquired with FT resolution of 15,000. Normalized collision energy was set to 33 and already targeted precursors were dynamically excluded for further isolation and activation for 15 sec with 5 ppm mass tolerance.

MS data processing quantification and statistical analysis

Raw files were analyzed with Proteome Discoverer 1.4 software package (Thermo Finnigan), using the Sequest search engine and the Uniprot human (Homo sapiens) reviewed database, downloaded on December 15, 2017, including 20,243 entries. The search was performed using carbamidomethylation of cysteine as static and oxidation of methionine as dynamic modifications. Two missed cleavage sites, a precursor mass tolerance of 10 ppm and fragment mass tolerance of 0.05 Da were allowed. False discovery rate (FDR) validation was based on q value: target FDR (strict): 0.01, target FDR (relaxed): 0.05. Label free quantification was performed by utilizing the precursor ion area values exported from the total ion chromatogram as defined by the Proteome Discoverer v. 1.4.0.288 (Thermo Scientific).

In silico analysis

Pathway analysis was performed using the ClueGO/Cytoscape 3.5.1 software (http://apps.cytoscape.org/apps/cluego).[62] Ontologies were retrieved from the REACTOME pathway database (https://reactome.org/) and statistically significant pathways (Benjamini-Hochberg corrected p≤0.05, two-sided hypergeometric test) were evaluated. Analyses for biological functions, subcellular localization, cellular development and signaling of the output proteins were conducted by using Gene ontology (GO) (http://geneontology.org), Swiss-Prot (https://www.uniprot.org) databases and STRING software (https://string-db.org/). Proteins were clustered using Morpheus software (https://clue.io/morpheus). Three-D visualization of MFGE-8 expression in liver tissue was conducted using Imaris software (https://imaris.oxinst.com), while volcano plots were generated using the R software package.

QUANTIFICATION AND STATISTICAL ANALYSIS

The ANOVA test was used for statistical analysis. P-values are presented in the figures, where *p<0.05, **p<0.01, ***p<0.001 and ****p<0.0001. The non-parametric Mann-Whitney test was applied for the analysis of the proteomic data using SPSS software (IBM SPSS Statistics, NY: IBM Corp., 2013). Statistically significant proteins (p<0.05) with a fold change <0.67 and >1.5 were considered as downregulated and upregulated, respectively (t-test).

Protein expression levels were measured with ImageJ-win64.

Output files from Proteome Discoverer were processed with R programming language for statistical computing (version 4.0.3). The intensity of protein samples from each cell category was firstly normalized to the mean of average intensity of all proteins.